pCO_2 in the Mediterranean Sea during the cruise MSM 72

Master Thesis

In Chemistry

Department of Chemistry

Christian-Albrechts-University Kiel

Submitted by

Lennart Gerke

Kiel, February 2020

Erstgutachter: Prof. Dr. Arne Körtzinger
Zweitgutachter: Prof. Dr. Hermann Bange

Kiel, February 2020

The Master thesis was written

between September 2019 and February 2020

Supervision: Prof. Dr. Arne Körtzinger

Institute of Chemical Oceanography

Christian-Albrecht-University Kiel

Table of contents

Abbreviations

ADCP	Acoustic Doppler Current Profiler
AS	Adriatic Sea
AW	Atlantic Water
CRM	Certified Reference Material
CSW	Cretan Surface Water
CTD	Conductivity, Temperature and Depth
dbar	dezibar
DIC	Dissolved Inorganic Carbon
DO	Dissolved Oxygen
DShip	Davis-Ship
EMDW	Eastern Mediterranean Deep Water
EMS	Eastern Mediterranean Sea
EMT	Eastern Mediterranean Transit
e.m.f.	electromotive force
fCO_2	fugacity of carbon dioxide
i.e.	id est
kn	knots
LDW	Levantine Deep Water
LIW	Levantine Intermediate Water
LSW	Levantine Surface Water
MSM	Maria S. Merian
Med	Mediterranean Sea
MLD	Mixed Layer Depth
nm	nautical miles
NDIR	Non-Disperse Infrared
pCO_2	partial pressure of carbon dioxide
ppm	part per million
µatm	microatmospheres
µmol/kg	micromole per kilogram
SOMMA	Single Operator Multi-parameter Metabolic Analyzer
SOCAT	Surface Ocean Carbon Atlas
SST	Sea Surface Temperature

SSS	Sea Surface Salinity
TA	Total Alkalinity
TDW	Tyrrhenian Deep Water
TS	Tyrrhenian Sea
UTC	Coordinated Universal Time
uCTD	underway Conductivity, Temperature and Depth
VINDTA	Versatile Instrument for the Determination of total inorganic carbon and Titration Alkalinity
WMDW	Western Mediterranean Deep Water
WMS	Western Mediterranean Sea
WMT	Western Mediterranean Transit
xCO_2	mole fraction of carbon dioxide

Abstract

This thesis analyzed variations in the partial pressure of CO_2 (pCO_2) in different parts of the Mediterranean Sea (Med). pCO_2 data were recorded by continuous monitoring (underway measurements) during the cruise MSM 72 along an Ionian section (from Crete along the Greek coast until the Otranto Strait) and along a zonal section (from Crete to the Strait of Gibraltar). Different parameters affecting the pCO_2 values such as temperature, salinity and currents were also examined and taken into account.

The results showed a general undersaturation of the sea surface pCO_2 as compared to the atmosphere, which according to previous data was expected for the time of the measurements (March). pCO_2 levels stayed relatively constant in the open sea with levels in the Eastern Mediterranean basin slightly higher than those in the Western Mediterranean basin. The most significant pCO_2 variations were observed within the different straits along the two sections (Otranto Strait, Strait of Sicily, Strait of Sardinia and Strait of Gibraltar). This was particularly evident close to and in the Strait of Gibraltar, where pCO_2 also increased significantly as compared to the Western Mediterranean basin. This increase and the higher degree of pCO_2 variations were most likely caused by upwelling CO_2-rich water masses and currents/eddies that occurred in the Strait of Gibraltar and the neighboring Alboran Sea at the time of the cruise.

Zusammenfassung

In dieser Masterarbeit wurden Variationen im Partialdruck von CO_2 (pCO_2) in unterschiedlichen Regionen des Mittelmeers analysiert. Die pCO_2 Daten wurden auf der Schiffsreise MSM 72 durch kontinuierliche Messungen des Oberflächenwassers erhalten, zum einen entlang eines Abschnitts durch die Ionische See (von Kreta bis zur Otranto Straße) und zum anderen entlang eines zonalen Schnittes (von Kreta bis zur Straße von Gibraltar). Temperaturabhängige Einflüsse sowie mögliche Auswirkungen von Salzgehalt und Meeresströmungen auf den pCO_2 Gehalt wurden ebenfalls ermittelt und in der Analyse berücksichtigt.

Die Ergebnisse zeigten eine generelle Untersättigung des Mittelmeerwassers im Vergleich zum pCO_2 Gehalt der Atmosphäre, was für den Zeitraum, in dem die Messungen durchgeführt wurden (März), laut Literaturdaten zu erwarten war. Generell wurden in der offenen See relativ konstante pCO_2 Werte gemessen, wobei der CO_2 Gehalt im östlichen Mittelmeer leicht über dem im westlichen lag. Signifikante lokale Veränderungen im pCO_2 wurden in den Meerengen wie der Otranto Straße sowie den Straßen von Sizilien, Sardinien und Gibraltar beobachtet. Vor allem in der Straße von Gibraltar stieg der pCO_2 gegenüber den Werten im westlichen Mittelmeer beträchtlich an und es zeigten sich große Variationen, die vermutlich auf aufsteigende CO_2-reiche Wassermassen und Strömungen im angrenzenden Alboran-Meer zurückzuführen waren.

1. Introduction

1.1 The Cruise

This thesis studied the partial pressure of carbon dioxide (pCO_2) in different parts of the Mediterranean Sea. pCO_2 values at the ocean surface as well as other ocean parameters like transient tracers and nutrient concentrations (nitrite, nitrate, phosphate and silicate), salinity and temperature were measured during a cruise from Heraklion in Greece to Cadiz in Spain. The salinity, temperature and pCO_2 data were recorded on underway instruments during the entire cruise and the other parameters were measured in discrete samples taken at specific station. The cruise was carried out with the research vessel Maria S. Merian under the cruise number MSM 72 was lead by D. Hainbucher (IfMHH, Institut für Meereskunde in Hamburg) and included scientists from different countries (Germany, Spain, Italy, Greece and Lebanon). MSM 72 took place between the 2nd March and the 3rd April, 2018, and covered a zonal section through the Mediterranean Sea all the way from the east of Crete to the Strait of Gibraltar. In addition, an Ionian section from the west of Crete along the Greek coast into the Strait of Otranto was included (see figure 1). During the zonal section discrete samples were collected at 108 stations starting at a longitude of 26 °E and ending at a longitude of 6 °W, with the latitude changing between 34 °N and 38 °N. The Ionian section covered a slightly larger latitude change from 34 °N to 40 °N and included 26 measuring stations.[1]

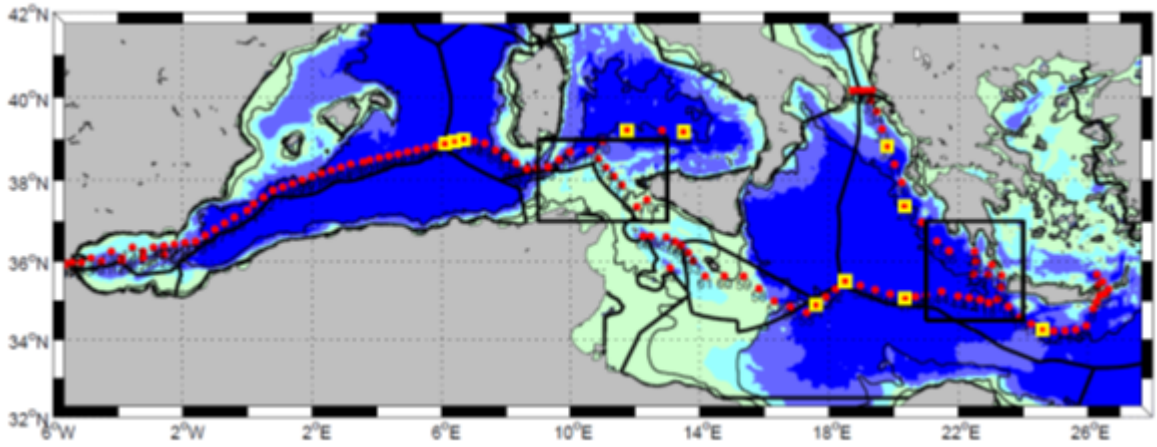

Figure 1: Map of the different measuring stations during cruise MSM 72 through the Mediterranean Sea. The red dots show the CTD (Conductivity, Temperature and Depth) stations. Stations marked in yellow highlight positions where Argo floats were deployed into the sea. Black squares mark areas where Acoustic Doppler Current Profiler (ADCP) and underway Conductivity, Temperature and Depth (uCTD) measurement sequences were carried out.[2]

Due to political issues, underway measurements and discrete samples could not be obtained in the eastern part of the Eastern Mediterranean Sea, specifically in the Levantine basin. Along the zonal section, new measuring stations were set up every 15 nm (nautical miles) and samples were collected. As some parameters such as transient tracers, Dissolved Oxygen (DO), pH and alkalinity required longer analysis times between stations they were only measured in water samples of every second station. On the other hand, values for temperature, salinity and conductivity at different depths could be obtained at every station providing a detailed catalogue of these values in the zonal and Ionian sections of the cruise.[1]

1.2 Water masses in the Mediterranean Sea

The Mediterranean Sea (Med) is located between the continents Europe, Africa and Asia. It is a semi-enclosed Sea, which is connected to the Atlantic Ocean via the Strait of Gibraltar and to the Indian Ocean via the Suez Canal. Its boundaries are Europe to the north with the countries Spain, France, Italy, Slovenia, Croatia, Albania, Greece and Turkey, Asia to the east with Syria, Lebanon and Israel, and Africa to the south with Egypt, Libya, Tunisia, Algeria and Morocco. It covers a surface of approximately

3 Mio. km^2, roughly 0.8 % of the world's ocean surface, and has an average depth of 1500 m. The deepest spot is located in the Ionian Sea with 5267 m.[3,4]

The Med can be divided into three major circulation cells, one shallow circulating across the entire Mediterranean at the level of the zonal section covered by this cruise and two deep overturning circulations, one occurring in each basin, the Western Mediterranean and the Eastern Mediterranean basin. The Med is considered one of the most complex marine environments. This is due to many physical processes occurring in the water, including thermohaline circulations, gyres and the formation of deep-water. Different water masses flow through the Mediterranean Sea and its different basins (see figure 2).[4,5]

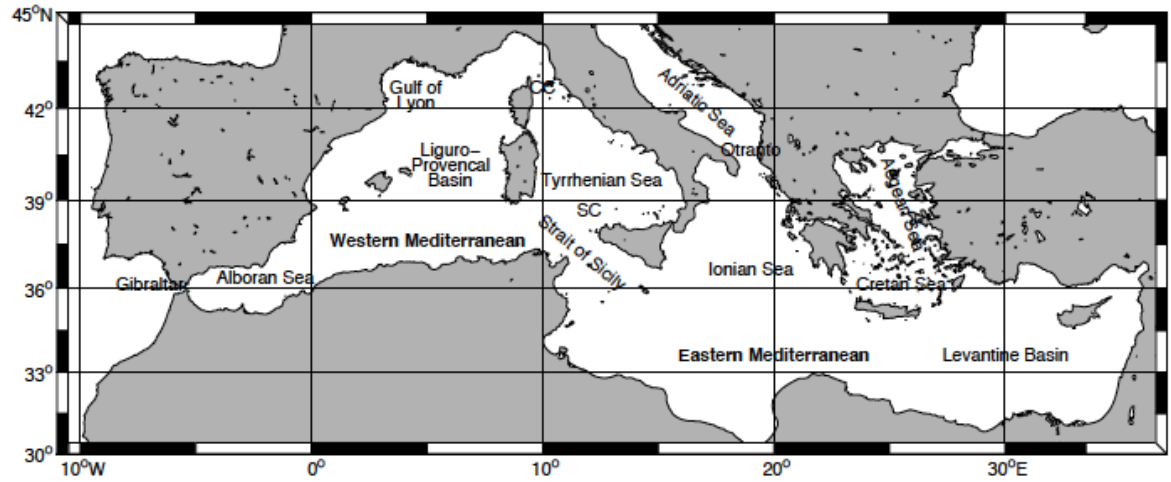

Figure 2: Map of the Mediterranean Sea with the different basins.[6]

Open ocean water enters the Med mainly through the Strait of Gibraltar and travels eastward at the surface. This water mass is called Atlantic Water (AW) and is characterized by low salinity and low alkalinity. The AW flows along the African coast becoming more and more saline and dense on its way towards the Strait of Sicily; this change is caused mainly by evaporation. Before the Strait of Sicily the AW separates; one part travels further east into the Eastern Mediterranean Sea (EMS) and the Levantine basin while the other part enters the Tyrrhenian Sea. In the north, this second branch moves back into the Balearic Sea through the Corsica Channel and closes its circle in the Alboran Sea where the fresh AW arrives. Following the Strait of Sicily the AW that had entered the EMS splits up again. The major part continues flowing east towards the Levantine basin till the shores of Lebanon and Israel, becoming more saline due to further evaporation. Another smaller part of the AW flows north into the Ionian Sea and

then further into the Adriatic Sea. In the EMS, the incoming AW is found at depths of 50 m to 100 m. In the Levantine basin, a thin water film called the Levantine Surface Water (LSW) is present on top of the AW, which is characterized by the highest temperature and salinity of the entire Med.[5,7,8]

In the far east of the EMS, in the Rhodes Gyre, the AW has reached its maximum density due to intense surface water evaporation and thus sinks to lower depths forming the Levantine Intermediate Water (LIW). This water mass is one of the major reasons for the thermohaline circulation in the Mediterranean Sea. Although most of the water sinks to lower depths in the Levantine basin, some parts of the AW continue flowing north through the Cretan and Aegean Sea.

The warm and salty LIW, which is located at depths between 300 and 700 m, travels west and thus back towards the Atlantic Ocean, becoming less saline on its way due to mixing with other water masses. Some parts of the LIW also flow northward through the Ionian Sea into the Adriatic, but the major part moves towards the Sicily Channel. Below the eastern moving AW the LIW enters the Tyrrhenian Sea (TS) at the Strait of Sicily and during its movement through the TS becomes colder and less salty. It enters the western Basin of the Med (WMS) mainly through the Strait of Sardinia but also through the Corsica Channel into the Gulf of Lyon. The main part of the LIW then flows out into the Atlantic Ocean through the Strait of Gibraltar at depths below 250 m. The two water masses, AW and LIW, are the main components of the shallow circulation of the Med.[5,7,8]

Deep water masses are also formed in each basin and drive the deep overturning circulations in the Med. The Eastern Mediterranean Deep Water (EMDW) is mainly formed in the Adriatic Sea (AS), specifically in the northern part of the AS due to a downwelling of surface waters driven by continental shelves, and in the southern part of the AS due to open ocean convection. The two deep Adriatic water masses mix and enter the Ionian Sea through the Otranto Strait. In the eastern part of the Levantine Basin where the LIW is formed, further sinking of the water leads to the generation of the Levantine Deep Water (LDW). The two deep water masses described above, the Deep Adriatic Water and the LDW, mix within the eastern basin forming the EMDW. A small part of this water mass enters the Tyrrhenian Sea below the LIW, the rest stays inside the eastern basin.

The Western Mediterranean Deep Water (WMDW) is formed in winter in the Gulf of Lyon. Cold air and high winds mix the AW and the warmer and saltier LIW, which leads

to a heat loss and further sinking and thus the formation of the WMDW. The WMDW mainly stays inside the western basin but a small part also enters the Tyrrhenian Sea below the outflowing LIW at the Sardinia Channel. Here it mixes with the incoming EMDW and some LIW generating the Tyrrhenian Deep Water (TDW). This water mass cycles through the Tyrrhenian Sea and partly returns into the western basin against the inflowing WMDW at the Sardinian Channel.[5,7,8]

In the early 1990's one event, called the Eastern Mediterranean Transit (EMT), affected the deep water formation and thermohaline properties in the Eastern Mediterranean Sea, leading to increased and more rapid EMDW formation. Unusually cold conditions occurred in the Cretan and Aegean Sea and the saltier water sank to further depths at this point. These special conditions shifted the main formation of the EMDW abruptly into the Aegean and Cretan Sea. By now the condition have returned back to normal and the main deep water formation again occurs in the northern and southern part of the Adriatic Sea.[6]

In the mid-2000's (2004-2006), a similar event took place in the western basin, called the Western Mediterranean Transit (WMT). Again an unusually high amount of deep water was formed due to extreme winters. This resulted in anomalously warm waters with high salinity in deep parts of the western basin. The WMT is considered less significant than the EMT, but it might have been caused by the EMT.[6]

1.3 CO_2

Carbon Dioxide (CO_2) is a linear, colorless and odorless gas, which consists of one carbon atom and two oxygen atoms (see figure 3).[9]

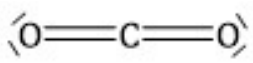

Figure 3: Chemical structure of CO_2.

The gas is present in the earth's atmosphere where its concentration in preindustrial times has been balanced mainly due to metabolic production and consumption in organisms and air-sea gas exchange; it has toxic features at high concentrations of more than 20000 ppm as compared to normally 400 ppm in air.[9,10]

In the preindustrial time the atmosphere contained approximately 180 to 300 ppm of CO_2 remaining relatively constant over hundreds of thousands of years, before sharply increasing to about 390 to 410 ppm from 1960 until now (see figure 4). This significant increase is a result of anthropogenic CO_2, i.e. CO_2 emissions caused by human activities, especially the burning of fossil fuels such as oil and coal.[11]

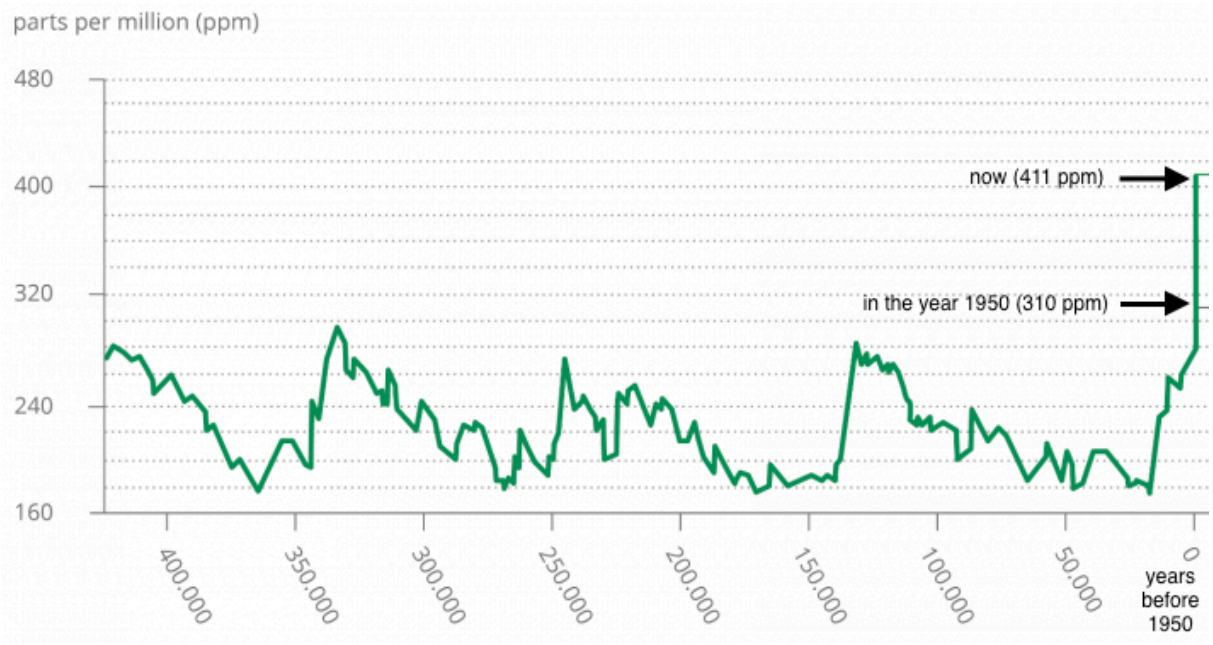

Figure 4: CO_2 concentration in the atmosphere in the last 400000 years.[12]

CO_2 and also anthropogenic CO_2 of the atmosphere enter the oceans mainly via air-sea gas exchange.

1.3.1 Air-sea gas exchange

At the interface between air and sea, atmospheric gases including CO_2 can enter the ocean water. Air-sea gas exchange represents a major mechanism of how gases from the atmosphere enter the oceans, dissolve in water and vice versa how dissolved gases leave the water. Air-sea gas exchange can occur by evaporation, bubble production and wave breaking.

The rate at which each gas enters or leaves the ocean via air-sea gas exchange is described via its flux (F). Flux can only occur when a gradient between the partial pressure of the gas dissolved in the water and the gas in the atmosphere exists. When

the sea is oversaturated (with respect to the atmosphere), efflux will occur whereas gas will enter the water when the sea is undersaturated for the respective gas.
Mathematically, the flux can be described as a product of gas transfer velocity (k_G) and thermodynamic force ($\mathbf{\Delta}C$) (see equation 1).[13,14]

$$F = k_G * \Delta C \quad \mathbf{1}$$

The thermodynamic force ($\mathbf{\Delta}C$) results from the concentration gradient and can be described as the difference in concentration for the respective gas between sea and atmosphere (see equation 2).[14]

$$\mathbf{\Delta}C = [Gas_{air}] - [Gas_{sea}] \quad \mathbf{2}$$

The concentration inside the water phase is determined by the solubility in water and the partial pressure of each gas above the water. The partial pressure is calculated by multiplying the mole fraction of the gas (xGas) with the total pressure of the gas mixture (p) in dry air (see equation 3).[15]

$$pGas_{air} = xGas * p \quad \mathbf{3}$$

The concentration of the gases inside the water phase is then determined with the help of Henry's law, where H_G is the gas specific proportionality Henry constant between the partial pressure of the gas above the solution ($pGas_{air}$) and the concentration of the gas inside the solution ([Gas]) (see equation 4).[15]

$$[Gas_{sea}] = H_G * pGas_{air} \quad \mathbf{4}$$

The solubility of each individual gas is affected by different factors, for example the molecular weight of the gas molecule, the water temperature and the salinity. Among these factors the water temperature has the largest influence. Simplified, these effects can be summarized as follows:
- The colder the water, the higher the solubility of the gas.
- For non-reactive gases, such as noble gases, a higher molecular weight is linked to higher solubility.

- The higher the salinity, the lower the solubility.
- The heavier the gas molecule, the higher is the percentage change in solubility by changing temperatures.

The other parameter defining the flux, the gas transfer velocity (k_G), determines how fast gases enter and leave the seawater. This factor can be calculated by a specific constant for each gas (D_G) divided by the thickness of the boundary layer (δ_W) air-sea gas exchange takes place. The thicker this layer is, the slower is the exchange (see equation 5).[14]

$$k_G = \frac{D_G}{\boldsymbol{\delta_W}} \qquad \mathbf{5}$$

The thin layer where molecular diffusion occurs is typically considered 0.03 cm in the water and 0.3 cm in the atmosphere thus comprising only a tiny part when considering the entire size of atmosphere and ocean.[15]
Unperturbed (ideal) diffusion of the gas molecules at the air-sea interface can only take place when no turbulences occur in the boundary layers. This is almost never the case, due to waves and winds. Thus, it is almost impossible to precisely calculate the gas transfer velocity and thereby the flux of each gas. Calculation methods have been developed, which attempt to determine gas transfer velocities in non-ideal conditions taking into account measured wind speeds and the Schmidt number for turbulent mass transport (calculated by dividing the kinematic viscosity of seawater by the diffusion of the gas in seawater at specific temperature and salinity). However, this only delivers satisfying results for wind speeds below 15 m/s.[14,16] At higher wind speeds the calculated gas transfer velocity has high errors. Another problem for calculating the diffusion by taking wind speed into account relates to the place where this speed is measured. Usually measurements occurs on top of the research vessels at approximately 10 m above sea level, where no friction due to contact with the water surface occurs. This introduces another error into the calculation. Alternative techniques to measure gas transfer velocities have been developed, involving for instance wind/wave tanks or purposefully release tracers, but none deliver satisfying results until now.[13]

1.3.2 CO_2 system in the ocean

When gas molecules of CO_2 enter the seawater, approximately 1 in 650 to 1000 molecules reacts with the water to form carbonic acid as defined by the hydration equilibration constant (see equation 7). The pH of the water then determines the status of the hydrated carbon, i.e. the relative fraction of carbonic acid, hydrogen carbonate and carbonate as defined by the first and second dissociation constants of carbonic acid (see equations 8&9).[17]

$CO_2(g) \overset{K_0}{\rightleftharpoons} CO_2(aq)$	air-sea gas exchange	**6**
$CO_2(aq) + H_2O(l) \overset{K_H}{\rightleftharpoons} H_2CO_3(aq)$	reaction with water	**7**
$H_2CO_3(aq) \overset{K_1}{\rightleftharpoons} H^+(aq) + HCO_3^-(aq)$	pH dependent	**8**
$HCO_3^-(aq) \overset{K_2}{\rightleftharpoons} H^+(aq) + CO_3^{2-}(aq)$	pH dependent	**9**

Due to the fact that CO_2 (aq) and H_2CO_3 (aq) cannot be differentiated easily by analytical measurements of the water, they are often combined to one species (CO_2^*).
The Bjerrum-Diagram describes the pH-dependent formation of the different carbonic acid species (see figure 5).

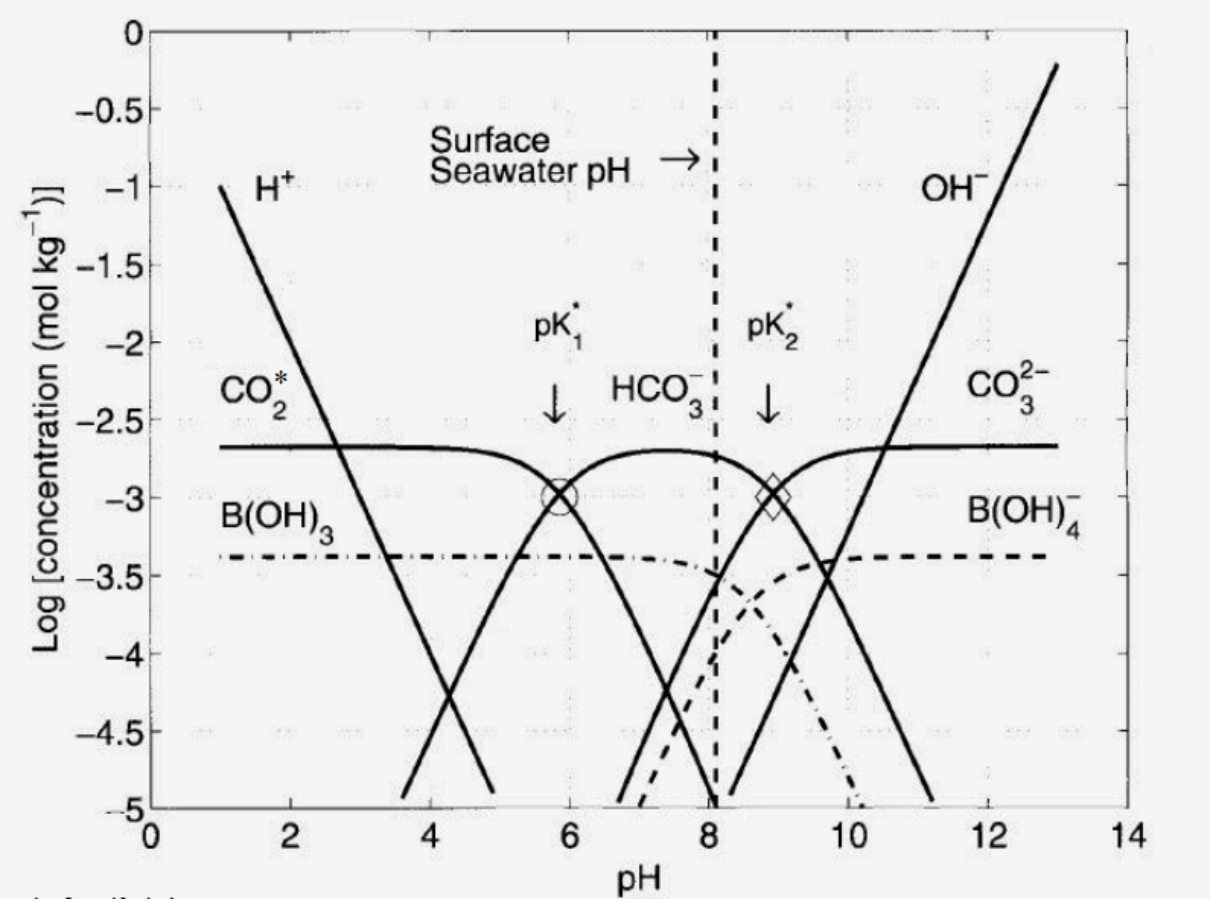

Figure 5: Bjerrum-Diagram showing the concentration of different carbon and boron species as a function of pH.[18]

The oceans surface normally has a pH between 7.5 and 8.2, which results in a ratio of approximately 90:10:1 for HCO_3^-:CO_3^{2-}:CO_2^*. pH, i.e. proton concentration, is the most important factor affecting the equilibrium in equations 8 and 9 at a given CO_2^* concentration. However, as the equilibrium constants are temperature-dependent, the temperature of the water also plays a significant role in defining the fraction of hydrated carbon and respective carbonate species; the warmer the water, the lower the solubility constant (K_0) but the higher the dissociation constants (K_1, K_2) (see figure 6).

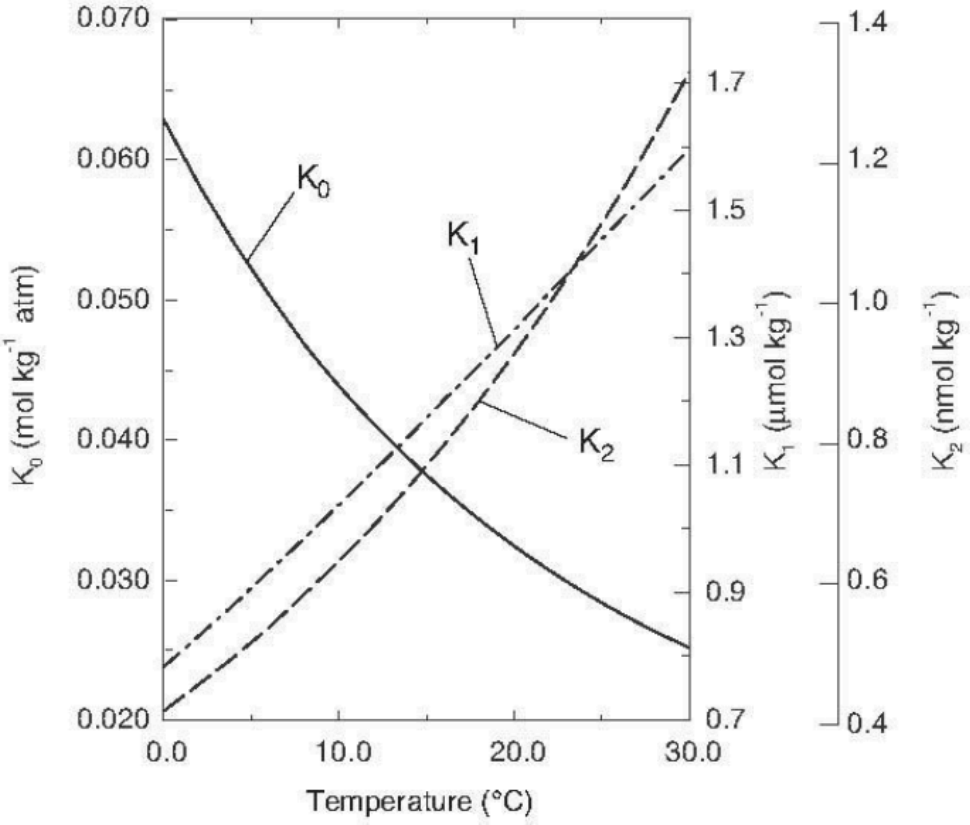

Figure 6: Diagram showing the temperature dependence of the dissociation constants K_1 and K_2 and the solubility constant K_0 (see equations 6, 8, 9).[19]

The dissociation constants K_1 and K_2 as well as the equilibrium constant for the hydration of CO_2 (K_H, equation 7) also vary with salinity and pressure of the environment although the effect of these parameters is less pronounced as compared to that of temperature. Typically, the dissociation constants K_1 and K_2 increase with salinity and pressure.

Four different measurable parameters are relevant for the marine CO_2-System. First, the partial pressure of CO_2, which is defined by the quotient of total CO_2^* concentration in the water over the solubility constant and governs the air-sea equilibrium and exchange (see equation 10).[17]

$$pCO_2 = \frac{[CO_2^*]}{K_0} \qquad \mathbf{10}$$

The concentration of the gas in the water is calculated as described above with the help of Henry's law (see equation 4).

The second parameter is the total Dissolved Inorganic Carbon (DIC), which represents the sum of the concentration of all dissolved carbon species in the water (see equation 11).[17]

$$DIC = \sum CO_2 = [CO_2^*] + [HCO_3^-] + [CO_3^{2-}] \quad \textbf{11}$$

Total Alkalinity (TA) is the third measurable parameter, which describes the acid binding capacity of the examined water. It is defined as the "number of moles of hydrogen ions equivalent to the excess of proton acceptors over proton donors" (Dickson, 1981). In seawater, TA is usually defined by the proton acceptors and donors given in equation 12.[17]

$$TA = [HCO_3^-] + 2[CO_3^{2-}] + [B(OH)_4^-] + [OH^-] + [HPO_4^{2-}] + 2[PO_4^{3-}] + [SiO(OH)_3^-] + [NH_3] + [HS^-] - [H^+] - [HSO_4^-] - [HF] - [H_3PO_4] \quad \textbf{12}$$

The last measurable parameter is the pH value, i.e. the negative decadal logarithm of protons present in the water (see equation 13). It describes the acidity of the seawater.[17]

$$pH = -\log [H^+] \quad \textbf{13}$$

With two of these four parameters given, the others can be calculated (see chapter 2.2.4). However, the calculation of DIC and TA from measured pCO_2 and pH values shows high errors with up to ± 20 µmol/kg as compared to approximately ± 3-4 µmol/kg when, for example TA is calculated using pH and DIC.[20]

It should be noted that the uptake of CO_2 differs from seawater to the (fresh) water of rivers and lakes and finally pure water. The ocean shows higher uptake capacity due to its good buffering that results from high concentration of CO_3^{2-}, the driving factor of the buffer capacity.

Fractional changes in pCO_2 are related to those in DIC multiplied by a constant factor, the Revelle factor (B) (see equation 14).

$$\frac{\delta pCO_2}{pCO_2} = B * \frac{\delta \mathrm{DIC}}{DIC} \qquad \textbf{14}$$

The larger the Revelle factor, the smaller is the uptake capacity of the respective water for CO_2. In the ocean, the Revelle factor varies between 8 and 15, mainly depending on the temperature of the ocean water. In cold waters, where the solubility of CO_2 is the highest, the Revelle factor is also high and thereby the uptake capacity itself is smaller (see figure 7).

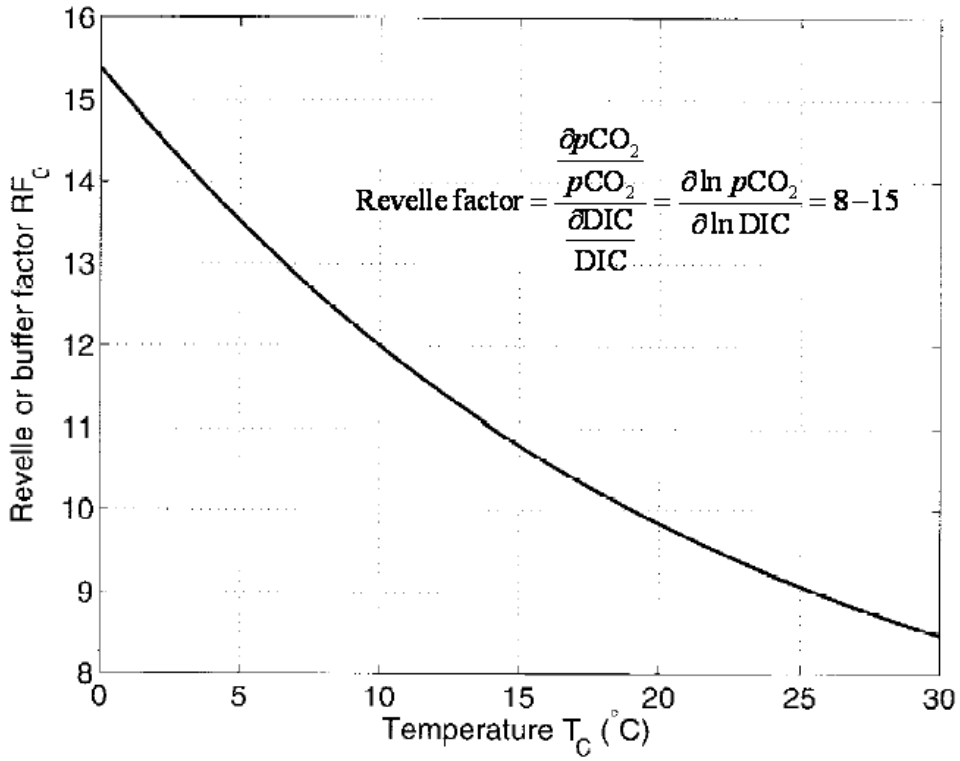

Figure 7: Diagram of the relationship between the Revelle factor and the temperature.[18]

Relatively high amounts of CO_3^{2-} in the ocean are an important determinant of the buffering capacity of the oceans as they act by binding the proton generated in the dissociation reaction of H_2CO_3 (see equations 8&9). However, this CO_2 buffering capacity of the ocean decreases with increasing CO_2. Higher CO_2 concentrations shift the pH of the seawater to lower values and thus cause acidification. With decreasing buffer capacity the ocean will take up and dissolve less CO_2 from the atmosphere, which leads to an even faster increase in the atmospheric CO_2 concentration. A resulting reduced amount of carbonate will also affect calcifying organisms (coral, plankton), as it becomes more difficult for them to form shells and skeletons.

2. Methods

2.1 Measurement of different seawater parameters

2.1.1 Dissolved Inorganic Carbon

Dissolved inorganic carbon (DIC), was measured with a Single Operator Multi-parameter Metabolic Analyzer (SOMMA). This instrument was designed by Johnson et al. (1993) and operates on the basis of coulometry as described below.[21]
A known amount of the seawater to be analyzed, is applied to a stripping chamber and acidified to move the equilibrium to the CO_2^* side (see equation 15).[22]

$$CO_3^{2-}(aq) + H^+(aq) \leftrightharpoons HCO_3^-(aq) + H^+(aq) \leftrightharpoons CO_2^* \qquad \textbf{15}$$

The chamber is then purged with a CO_2-free carrier gas, which absorbs the CO_2 gas molecules and is thereafter transferred into a solution of ethanolamine inside a coulometer. Here, the hydroxyethylcarbamic acid formed is titrated and the pH change of the solution is measured via transmittance. The hydroxide ions generated at the platinum spiral cathode by electrolyzing water form water with the hydrogen ions resulting from the titrated solution. Silver reacts at the anode to generate electrons (see figure 8).[22]

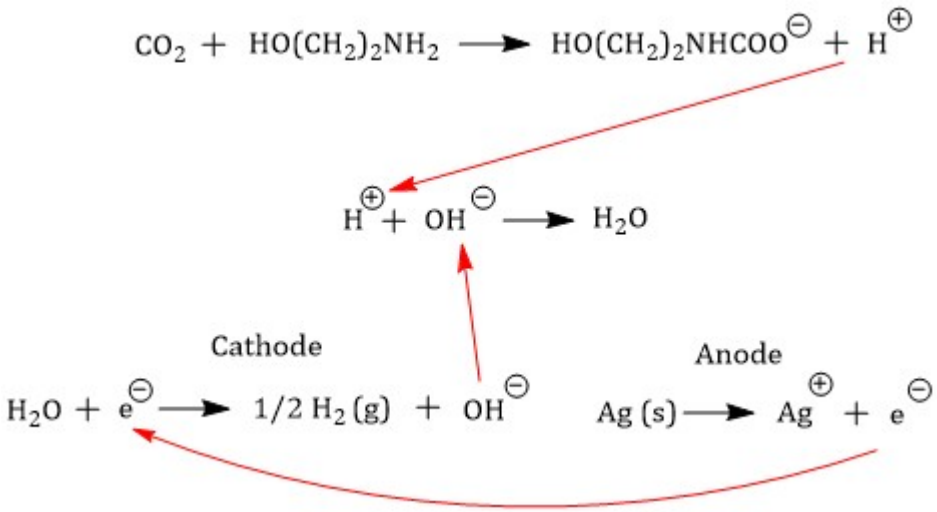

Figure 8: Different reactions occurring during the determination of DIC by coulometry. Top shows the formation of hydroxyethylcarbamic acid, middle the formation of water with the protons generated in the first reaction, and bottom reactions occurring at the cathode and anode.[22]

2.1.2 Total Alkalinity

Total Alkalinity (TA) is defined as follows (see equation 16):

$$TA = [HCO_3^-] + 2[CO_3^{2-}] + [B(OH)_4^-] + [OH^-] + [HPO_4^{2-}] + 2[PO_4^{3-}] + \ldots - [H^+] \quad \textbf{16}$$

In addition to the proton acceptors mentioned explicitly in the equation other proton acceptors exist in seawater, but their concentrations are so low that their influence is negligible (they are included as dots … in equation 16).[22]

TA was measured by determining the amount of acid needed to adjust the water sample to a specific pH, thus until all proton acceptors reacted with hydrogen ions. This can be performed in two different ways:

The first method for determining TA is based on a system called VINDTA (Versatile Instrument for the Determination of total inorganic carbon and Titration Alkalinity). It works as follows: An exact amount of seawater is injected into a measuring cell, where it is titrated with the help of hydrochloric acid. The titration uses a glass electrode pH cell to reveal the results. The solution of hydrochloric acid contains sodium chloride to adjust the ionic strength to that of the seawater. The acid is added into the titration cell in small increments, and the volume of acid needed and the e.m.f. (electromotive force), measured with the glass electrode pH cell, are determined until a pH of 3 is reached.[22]

The alkalinity of a sample can also be measured with the help of the double end point potentiometric technique. Here, a known amount of seawater is placed into an open measuring cell and is titrated twice. First, HCl is added until a pH of approximately 3.5 – 4 is reached and thereafter, the titration is continued until pH 3. The solution is stirred the entire time to allow the CO_2, which is formed during the titration, to escape. The volume of acid added and the e.m.f of the glass electrode pH cell are determined, as in the closed cell method, to compute the total alkalinity.[22]

During cruise MSM 72, TA was determined using the double end point method. To control the accuracy of TA and DIC measurements and calibrate the measuring cells, Certified Reference Material (CRM) samples with known TA and DIC values were measured at certain intervals.

2.1.3 pCO2

Carbon dioxide in seawater was determined by its partial pressure (see equation 10).
The partial pressure of CO_2 in the water was measured via the partial pressure of CO_2 in air, which was equilibrated with the respective water phase. This can be done either with an equilibrator system inside an equilibrator chamber or with the help of a sensor and a membrane equilibration as described below.
In the equilibrator system the respective water sample taken at a specific depth is pumped into the equilibrator chamber, where the air above the water phase (headspace) equilibrates with the water phase. This sets the partial pressure of the air equal to the partial pressure of the water sample. The pCO_2 of the air is then determined by multiplying the mole fraction (xCO_2) with the total pressure at equilibrium in dry air (p) (see equation 17).[22] Due to the equilibration this reveals the partial pressure of CO_2 in the water.

$$pCO_2 = xCO_2 * p \qquad \textbf{17}$$

In the sensor-based measurement the water flows past a membrane containing pores that allow the gas to slowly diffuses through the membrane pores into a headspace. Again the partial pressure of the equilibrated air in the headspace is measured, after being pumped through an air cycle where it is dried.
On the cruise, the pCO_2 was recorded underway with a HydroC-CO_2 sensor of the company Kongsberg KM Contros Maritime, which operates based on the membrane diffusion principle. The concentration of these gas molecules was then measured with the help of an NDIR (Non-Disperse Infrared) measuring cell.
The HydroC-CO_2 sensor had a size of 37.6 cm in length and 9 cm in diameter (see figure 9).[23]

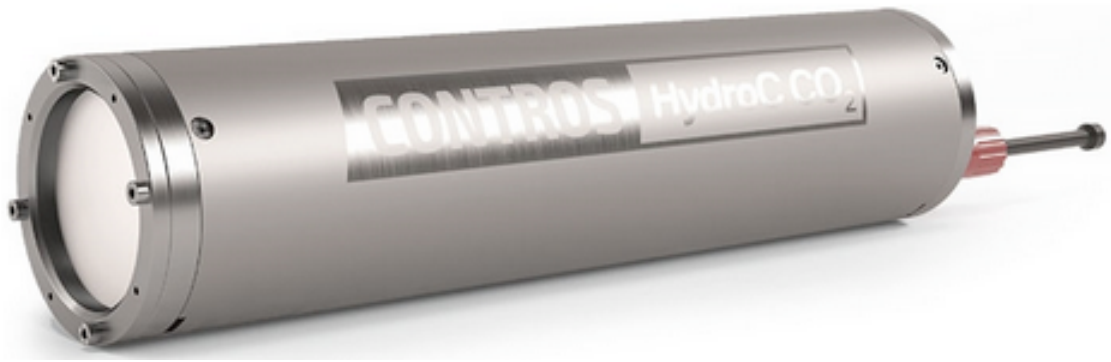

Figure 9: Picture of the HydroC-CO_2 sensor.[24]

CO_2 molecules absorb different wavelengths in a broad spectrum of infrared light in the range of 500 – 3800 cm^{-1} (see figure 10). One specific wavelength is monitored and the concentration of CO_2 is calculated from the absorbance at this wavelength.

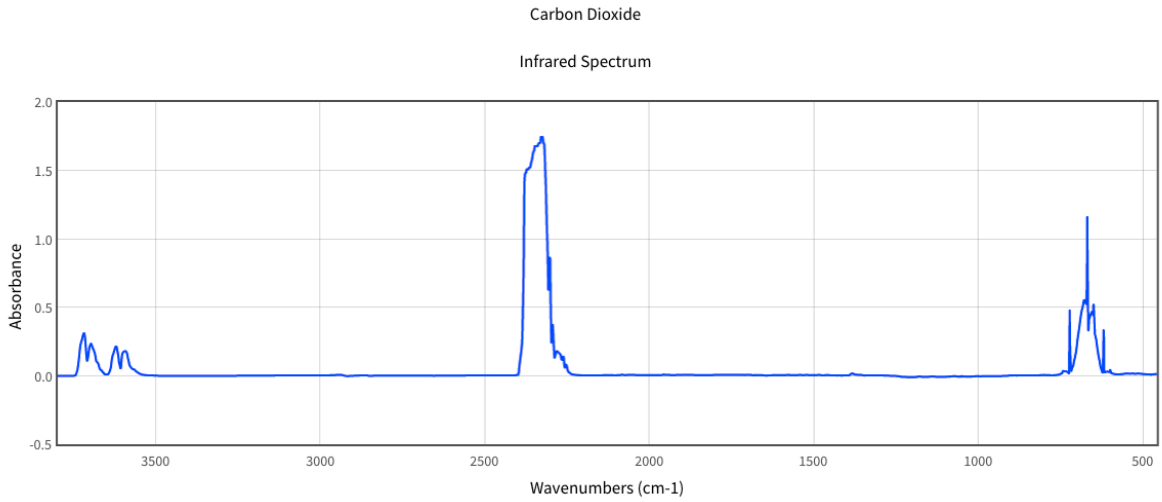

Figure 10: Absorption spectrum of CO_2.[25]

The sensor was located on deck of the ship in a cooling box, where surface water was continuously pumped through and temperature, O_2 and pCO_2 were measured. The water was taken from the centrifugal pump of the ship to obtain clean seawater. To measure the exact Sea Surface Temperature (SST) and Sea Surface Salinity (SSS) of the water, a SeaBird 5 salinity and temperature sensor was located at the intake position of the surface water.[1]

2.1.4 pH

The pH of specific water samples was determined by measuring the e.m.f. (electromotive force). This was compared to the e.m.f. of standard measurements using water samples with a known pH. The pH standard was composed of a TRIS (Tris(hydroxymethyl)-aminoethan)/HCl buffer and a 2-aminopyridine/HCl buffer in synthetic seawater. Both samples, the respective water sample and the calibration standard, were tempered to 25 °C and the pH was therefore generally expressed as pHT25.[22]

To calculate the insitu pH (pH_{insitu}), the change in temperature between the collected seawater and 25 °C has to be taken into account. This was done by subtracting the measured temperature of the water from 25 °C and multiplying this temperature difference by -0.01502 (Lui et al., 2017) (see equations 18&19).[26] This unveils the pH difference (pH_{diff}) caused by tempering the sample before the measurement.

$$T_{diff} = 25 - T_{measured} \quad \textbf{18}$$

$$pH_{diff} = T_{diff} * (-0.01502) \quad \textbf{19}$$

Finally, this pH difference (pH_{diff}) has to be subtracted from the measured pHT25 to obtain the final pH_{insitu} (see equation 20).

$$pH_{insitu} = pH_{T25} - pH_{diff} \quad \textbf{20}$$

2.1.5 Oxygen

Oxygen was measured with the help of an AADI Oxygen Optode 4330, located right next to the HydroC-CO_2 sensor inside the cooling box on deck of the research vessel. The oxygen concentration of the surface water, pumped into the cooling box, was determined with the help of a dynamic luminescence quenching method. The luminophore molecules, platinum porphyrin complexes, absorb light of a specific wavelength (505 nm) that is emitted from a blue-green light LED located inside the Optode. The photon absorption transforms the luminophore from its ground state into its excited state and the duration of this state is affected by the presence of oxygen molecules. If no oxygen is present in the water, the luminophore will slowly return to its

initial state by emitting photons of lower energy (red light). In case of oxygen present in the water and if the molecules collide, the luminophore will transfer some of its energy to the oxygen molecule and this results in emitting less photons of even lower energy and returning faster back to its ground state (see figure 11).[27]

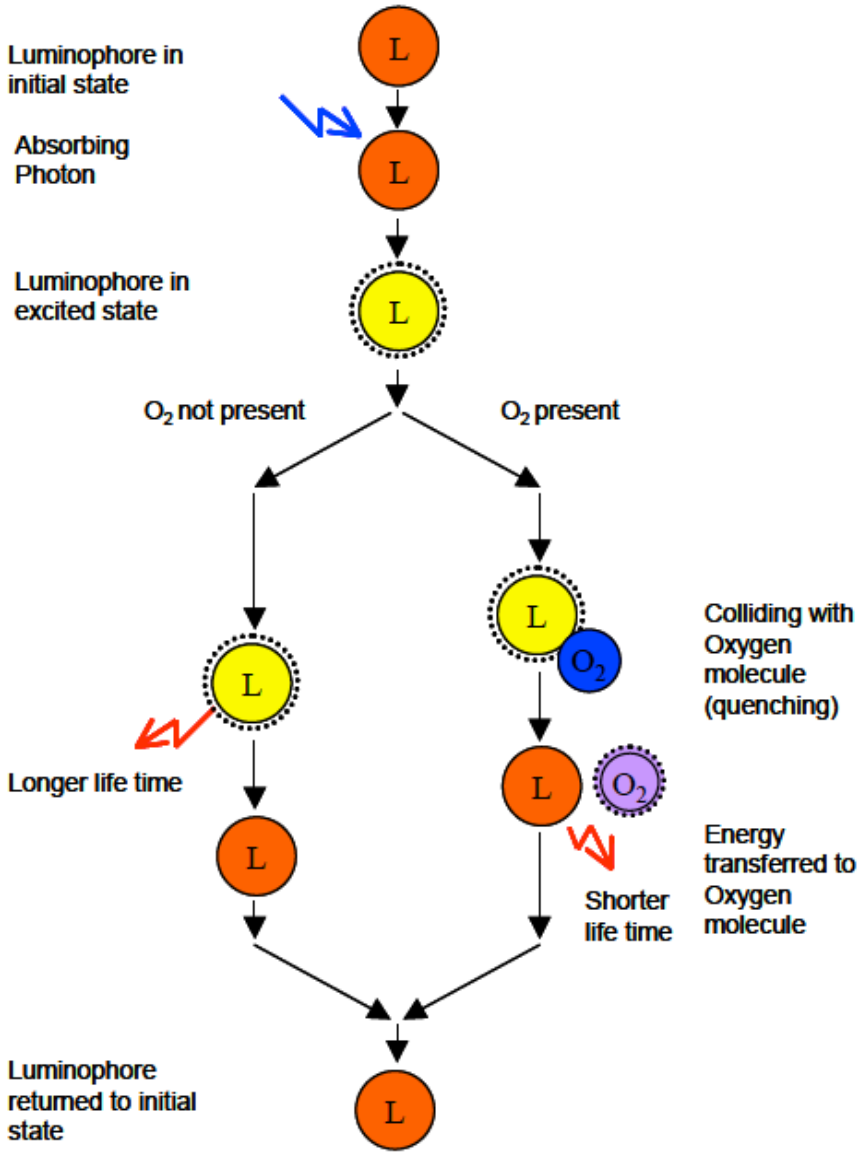

Figure 11: Principle of luminophore excitation and emission in the absence and presence of oxygen.[27]

The higher the oxygen concentration inside the water, the shorter is the lifetime of the luminophores in their excited state due to the likelihood of colliding with oxygen molecules. The intensity of the light emitted from the luminophores will also decrease; however, many other factors, like bleaching of the foil or optical coupling, have influence

on this intensity as well. This is the reason for mainly looking at the lifetime of the luminophores for calculating the oxygen concentration.[27]
The platinum porphyrin complexes are located in an indicator layer, which is only separated by an optical isolation layer from the surrounding seawater. This isolation layer has the function to protect the luminophores from influences like sunlight or other fluorescent materials inside the water. It is permeable to gas molecules but not to water, thus not affecting the concentration of oxygen molecules inside the water phase.[27]

2.1.6 Other parameters - salinity, oxygen, nutrients, carbonate, transient tracer

The salinity was measured at different depths with the help of a salinometer connected to the CTD, which was lowered into the interior of the sea at the different stations.[1]

All other parameters were measured in water samples, which were collected in Niskin bottles. These were lowered into the interior of the sea while connected to the CTD and collected water at the different depths.[1]

Oxygen of discrete samples was measured with the help of the automatic Winkler potentiometric method as described by Langdon (2010).[28] Briefly, manganese(II)-chloride, sodium-iodide and sulfuric acid were added to the respective water sample and the amount of iodine formed was measured by titration with sodium thiosulphate. The final dissolved oxygen values were reported in µmol/kg.[1,28]

Nutrients, also measured on board, were determined with a QuAAtro auto-analyzer from SEAL analytics (Germany) revealing the amounts of nitrite, nitrate, phosphate and silicate.[1]

The carbonate ion concentration (CO_3^{2-}) was determined spectrophotometrically using the method described by Patsavas et al. (2015).[1,29]

The transient tracers SF_6 and CFC12 were measured with the help of a Gas Chromatograph/Purge and Trap (GC/PT) system.[1]

2.2 Data Processing

2.2.1 Analysis of raw pCO_2 data

The CO_2 sensor measured almost during the entire cruise. Some technical issues were encountered and prevented measurements between the 6th and the 10th of March. Therefore, no results were obtained for the first part of the section through the Ionian Sea carried out at this time.

For calibration purposes the sensor was set to zero approximately three times per day. Each zero run took two minutes with a following flush of the sensor for 10 minutes until the system was ready to continue measuring the seawater pCO_2 values. At each zero run, data points were collected every ten seconds and during the flush even every five seconds. The relevant seawater pCO_2 values were measured after the flushes at one-minute intervals.

A zeroing of the sensor is required to calculate and reveal the drift of the sensor and take this into account for the measured data points. Data processing also involved a pre- and post-cruise calibration of the sensor, carried out by the company Contros itself.

Apart from other parameters, the sensor delivers a raw (S_{raw}) and a reference signal (S_{ref}) of the dual-beam NDIR measuring cell for all measured data points. Dividing the raw by the reference signal provides a referenced two-beam signal (see equation 21).[30,31]

$$S_{2beam} = \frac{S_{raw}}{S_{ref}} \qquad \mathbf{21}$$

This calculation was done once for all data points and once just for the points during each zero run (see equation 22). At every zero run the first 30 seconds (three data points) were flagged and not considered, because these showed higher values due to residual CO_2 being inside the sensor.[30,31]

$$S_{2beam,Z} = \frac{S_{raw,Z}}{S_{ref,Z}} \qquad \mathbf{22}$$

The drift-corrected NDIR signal was thereafter calculated by dividing the two beam signal for each point in time by the two beam signal of the zero for the respective time point (see equation 23).[30,31]

$$S_{DC}(t) = \frac{S_{2beam}(t)}{S_{2beam,Z}(t)} \qquad \mathbf{23}$$

To receive a zero value for each point in time, the zeros measured (see equation 22) were plotted against the runtime allowing interpolation in different ways: (1) interpolating linearly through all the data points (blue line in figure 12), (2) splitting the runtime and interpolating every part linearly but separately (green lines in figure 12), or (3) calculating a mean of the zero values from each zero run and interpolating from the mean of one zero to the mean of the next zero linearly (red line in figure 12).

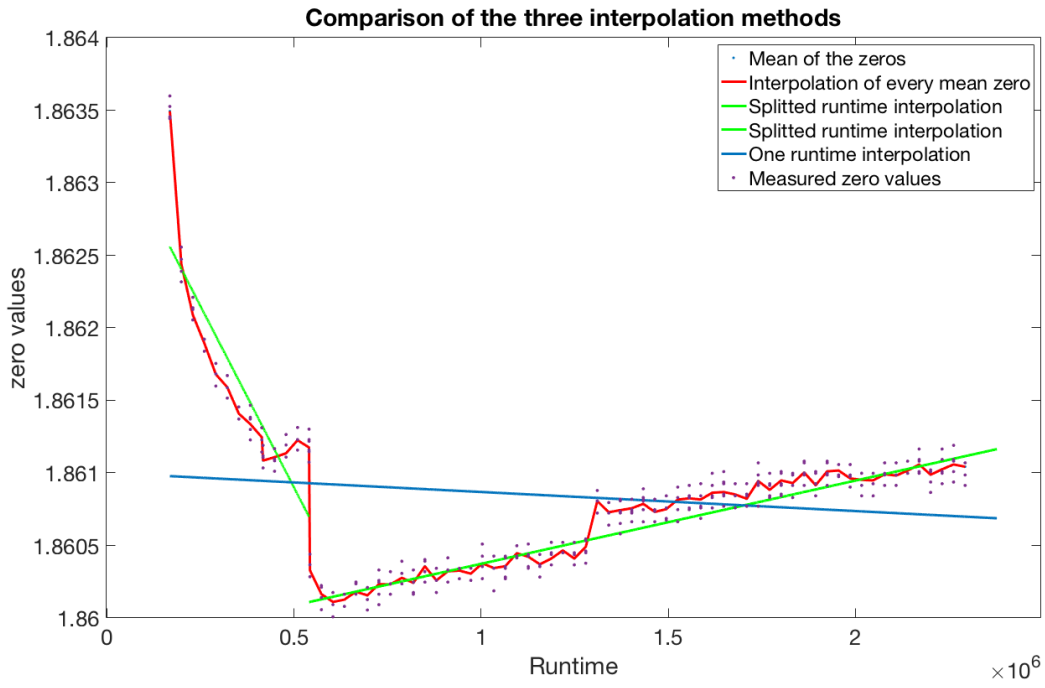

Figure 12: Display of the different interpolation methods to obtain a zero value for the pCO_2 quantification at each point in time. The blue line shows a linear interpolation through all zero data points, the green lines linear interpolations through the zero data with the runtime split into two, and the red line the interpolation from zero to zero for the mean of each zero run. The dots display the measured zero values (see equation 22).

As evident from figure 12, the linear interpolation through all zero values delivered inferior results with errors of up to ± 0.002 zero values. This is due to the zero values first decreasing significantly and then increasing slowly again.

The split runtime interpolation showed better results due to interpolating first the decreasing part linearly and then the slowly increasing part. For the second part this method delivered good results (± 0.0001 zero values) but for the first decreasing part the errors for each zero run are relatively large again (± 0.0005 zero values). The runtime could even be split into three parts, separating the second part at a runtime of 1.3 again. However, as the first declining part already shows the biggest errors, this was not taken into account.

The last interpolation method showed only minor errors because interpolation was performed from each zero to the next; however every zero itself had an error resulting from calculating the mean of 9 data points. Taking this into consideration, I chose the last interpolation method to achieve a zero for each point in time, because the error for each mean proved to be only ± 0.00008 zero values.

With the now calculated drift-corrected signal (see equation 23), the data analysis was continued. To obtain the final, processed signal of the NDIR sensor, the drift-corrected signal was multiplied by a NDIR unit-specific scale factor (F) after being subtracted from one (see equation 24).[30]

$$S_{proc}(t) = F(1 - S_{DC}(t)) \qquad \mathbf{24}$$

Finally, the pre- and post-cruise calibration values of the sensor were used to calculate calibration coefficients for each point in time from the resulting two beam signals of the zeros after the interpolation (see equation 25).[30] Each calibration delivered three calibration coefficients (k_1-k_3) due to the polynomial degree of the calibration function being three.

$$k_i(t) = k_{i,pre} + \left(\frac{S_{2beam,Z}(t_{first}) - S_{2beam,Z}(t)}{S_{2beam,Z}(t_{first}) - S_{2beam,Z}(t_{last})}\right) * (k_{i,post} - k_{i,pre}) \qquad \mathbf{25}$$

These calibration coefficients for each point in time ($k_1(t)$, $k_2(t)$, $k_3(t)$) were then used to calculate the mole fraction of carbon dioxide in wet air (see equation 26). The gas temperature (T_{gas}) and cell pressure (p_{NDIR}) were obtained from the data set and the

referenced gas temperature (T_0 = 273.15 K) and pressure (p_0 = 1013.25 mbar) represented standard values.[30]

$$x_{CO_2,wet}(t) = \left(k_3(t)S_{proc}^3(t) + k_2(t)S_{proc}^2(t) + k_1(t)S_{proc}(t)\right) * \left(\frac{p_0 * T_{gas}(t)}{T_0 * p_{NDIR}(t)}\right) \quad \textbf{26}$$

Thereafter, the partial pressure of CO_2 was calculated with the help of the pressure measured in the pressure sensor located behind the membrane (p_{in}) (see equation 27).[30]

$$p_{CO_2} = x_{CO_2,wet} * \frac{p_{in}}{1013{,}25} \quad \textbf{27}$$

Removing the zero and flush data from the final, calculated pCO_2 values revealed the relevant, drift-corrected and calibrated data measured during the cruise.

The final CO_2 data can be displayed as different physical parameters, either as the mole fraction, the partial pressure or the fugacity of CO_2. The mole fraction (xCO_2) depicts the 'number of moles of CO_2 divided by the sum of the number of moles of all constituents in a mixture in dry air' (see equation 28).[15]

$$xCO_2 = \frac{nCO_2}{\sum n_i - nH_2O} \quad \textbf{28}$$

To obtain the partial pressure (pCO_2), the mole fraction is multiplied by the total pressure minus the water vapor pressure (see equation 29).[15]

$$pCO_2 = xCO_2 * (P - pH_2O) \quad \textbf{29}$$

The fugacity (fCO_2) corresponds to the product of the partial pressure and an exponential function, which contains the first viral coefficient for CO_2 (B) and the cross viral coefficient (δ) (see equations 30-32). These two coefficients are temperature-dependent values.[15,22]

$$fCO_2 = pCO_2 * \exp\left(P * \left(\frac{B+2\delta}{RT}\right)\right) \quad \textbf{30}$$

$$B = -1636.75 + (12.0408 * T) - (3.27947e^{-2} * T^2) + 3.16528e^{-5} * T^3 \quad \textbf{31}$$

$$\delta = 57.7 - 0.188 * \mathrm{T} \quad \textbf{32}$$

Throughout this thesis, CO_2 concentrations in surface waters are given as pCO_2 values.

2.2.2 Flagging of pCO_2 data

To obtain high quality data and remove errors, some data points were removed from the original data set. These changes were indicated by flagging to provide clear information on the respective changes.[32] In the data set obtained during the cruise, seven adjustments were introduced. They are described here and in the following paragraphs. (1) One particular pCO_2 value was flagged and not considered. It showed an extremely high value of 1065.91 µatm, compared to the usual 300 to 450 µatm measured, indicating that some technical problem must have occurred. (2) Some changes were made and data flagged after carefully inspecting the DShip-data, which were provided by the research vessel and included parameters like intake temperature of the surface water, ship speed, etc. Around the 9th and 10th of March this temperature showed unrealistic values of 99.9990 °C. Therefore data points obtained on these days were removed from the data set. (3) Sudden increases or decreases in the DShip-temperature exceeding 1 °C per minute were also flagged. (4) Similarly, sudden changes in the Optode-temperature were flagged and the respective pCO_2 data not considered. Taken these considerations into account, the final data delivered a linear relationship between the temperature of the Optode measured in the cooling box next to the sensor and the DShip-temperature data measured at the seawater intake (see figure 13).

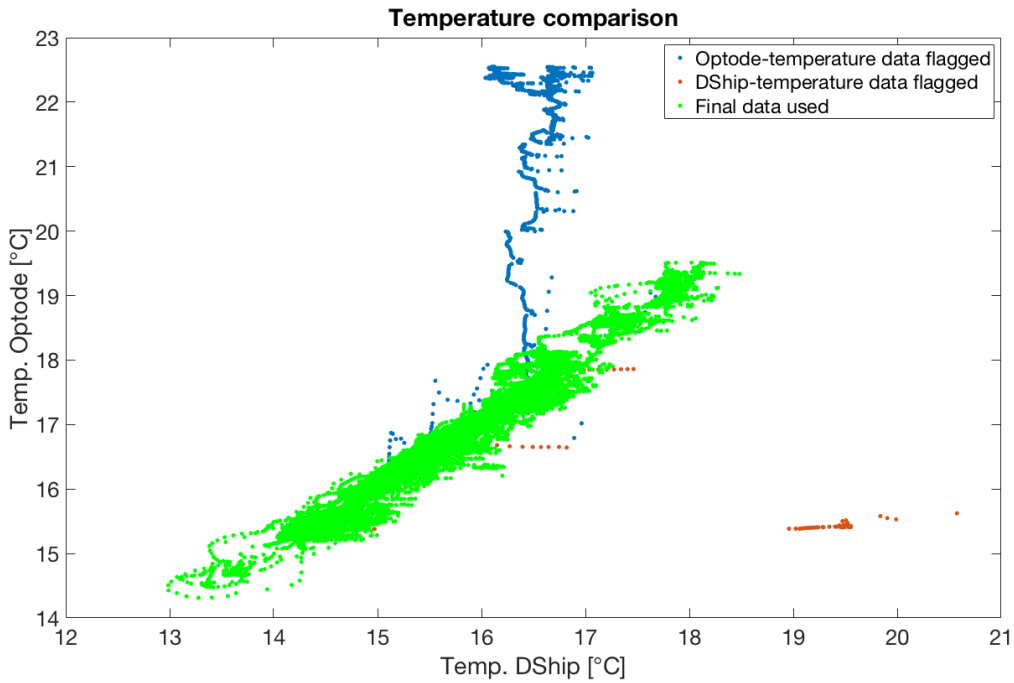

Figure 13: Relationship between the temperature of the Optode and the measured DShip-temperature. Green data points show the final dataset used, blue dots mark the flagged data characterized by a sudden increase or decrease in the Optode-temperature and red dots show the flagged data characterized by sudden changes in the measured DShip-temperature.

No such atypically rapid changes were seen in the DShip recordings of salinity and air-pressure and therefore no data were flagged here.

2.2.3 Shift of the Optode temperature

(5) The temperature of the Optode was shifted 3.5 minutes back in time to match it to the measured DShip-intake-temperature. This was done due to the fact that the water taken in from the surface of the Mediterranean had to be pumped towards the sensor and the time for this process had to be considered. The pCO_2 measured inside the sensor of course has to be connected to the temperature of the water at the position of the intake. To calculate the exact offset between intake and sensor, the measured temperature at the intake (DShip-temperature) and the temperature of the Optode were plotted against the time of the cruise and significant temperature increases and decreases in both temperature profiles were set to the same time (see figure 14). This resulted in a shift of the Optode-temperature of 3.5 minutes back in time.

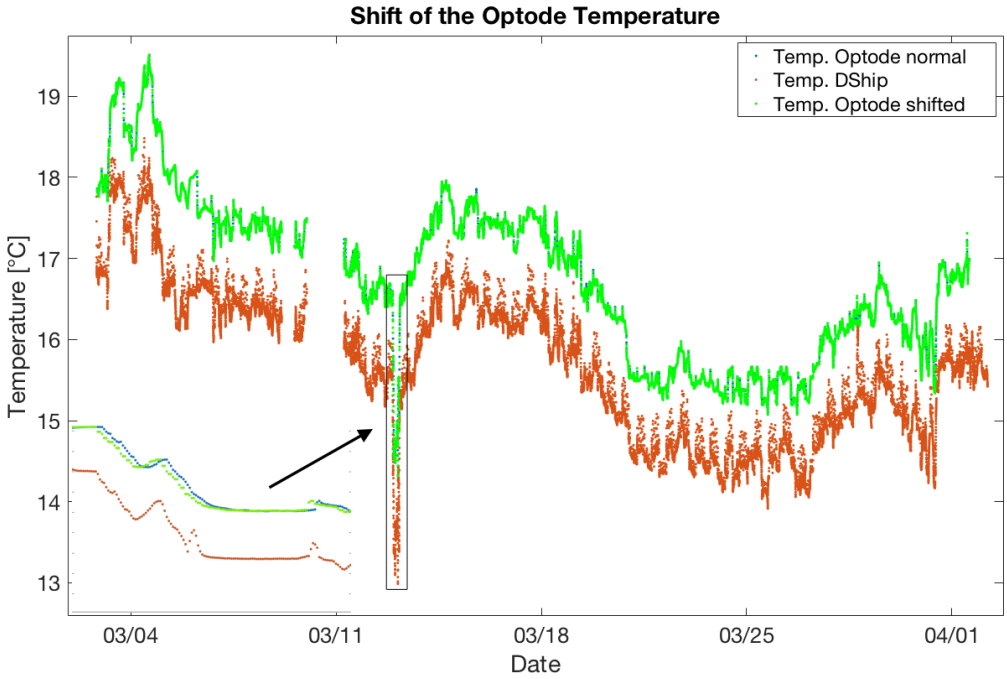

Figure 14: Diagram showing the offset of the Optode-temperature. A shift of 3.5 minutes back in time enabled a fit with the DShip-temperature. The red data points display the measured DShip-temperature at the intake, the blue values show the Optode-temperature and the green data points the shifted Optode-temperature. One part (around the 12th March) was zoomed in to show the shift of the Optode-temperature.

A remaining temperature offset of approximately 1 °C between the Optode and the DShip measurements was then included in the calculation of the final pCO_2 values (see equation 33).[22] This temperature difference probably results from the water warming up while being pumped from the surface towards the sensor. This change had to be considered because the solubility of CO_2 is strongly temperature-dependent and the pCO_2 at the intake (pCO_2 (T_{DShip})) is the relevant value.

$$pCO_2(T_{DShip}) = pCO_2(T_{Optode}) \cdot \exp\left(0.0423 \cdot (T_{DShip} - T_{Optode})\right) \qquad \mathbf{33}$$

2.2.4 Verifying the measured pCO_2 data

To verify data recordings with the sensor, discrete surface water samples were taken at different stations throughout the cruise and parameters measured in these samples (the first 10 m of each CTD cast) were compared to the sensor data. Therefore, the measured DIC, TA and pH values from these discrete samples were used to convert the

corresponding pCO_2 value. This was done using the software program CO2SYS (van Heuven et al., 2011) with the dissociation constants for carbonic acid (K1 and K2) from Luecker et al. (2000) and the HSO_4^- dissociation constant (K_{SO4}) from Dickson (1990).[33,34,35] Errors arising from the calculation were determined with the software program errors by (Orr et al., 2018) and also taken into account.[36] These corrected values of the individual discrete samples were then compared to the pCO_2 values measured by the sensor at the time of the sampling (see figure 15).

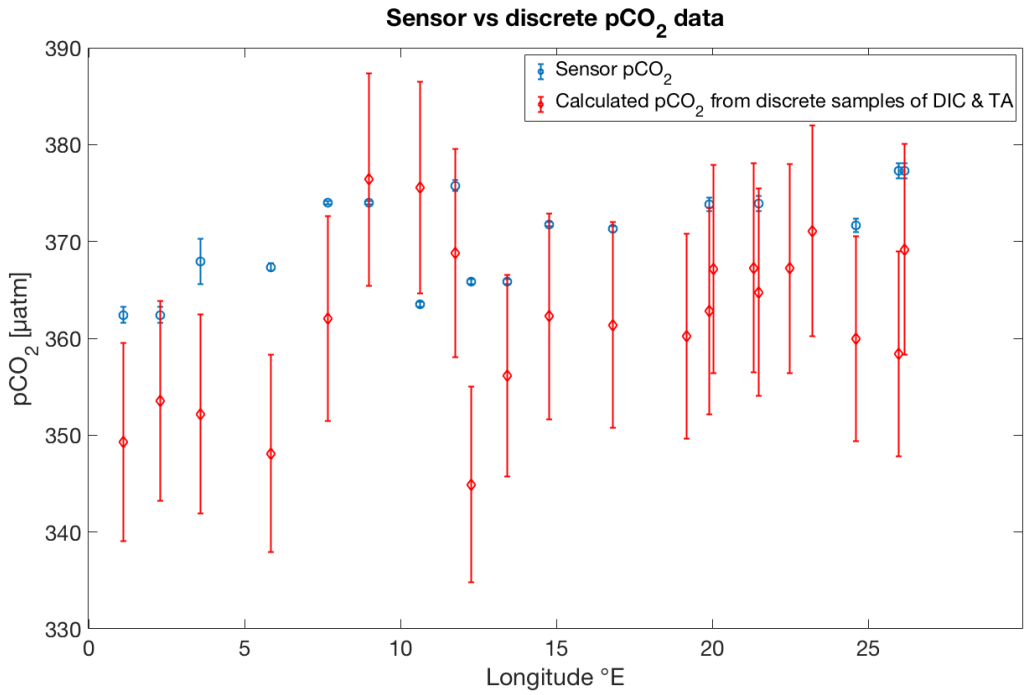

Figure 15: Mean of the sensor data (pCO_2) with standard deviation as error bars (blue) and the pCO_2 data calculated from the TA & DIC values measured in discrete samples taken at the respective longitude (red), also showing the errors in the calculation as error bars.

For the pCO_2 data measured in the sensor a mean of 10 minutes before and after the sampling was calculated and the standard deviation was taken into account as well. The results of the sensor data and the data calculated from the discrete samples agreed within 10 µatm.

2.2.5 Final flagging of pCO_2 data

A final look at the data revealed that at each station along the cruise, i.e. when the ship stopped at a given longitude and latitude, the sensor showed variations in the pCO_2

measurements within a range of 10-15 µatm. Most likely, this was due to the fact that the ship operated two pump jets, one in the front and one in the back, to hold the position during each station. These pump jets mixed the surface water and thereby had an influence on the measured pCO_2 values. (6) Therefore, data measured during pump jet operation were flagged and only data recorded when the ship had a speed of more than 2 kn (knots) were taken into account (see figure 16).

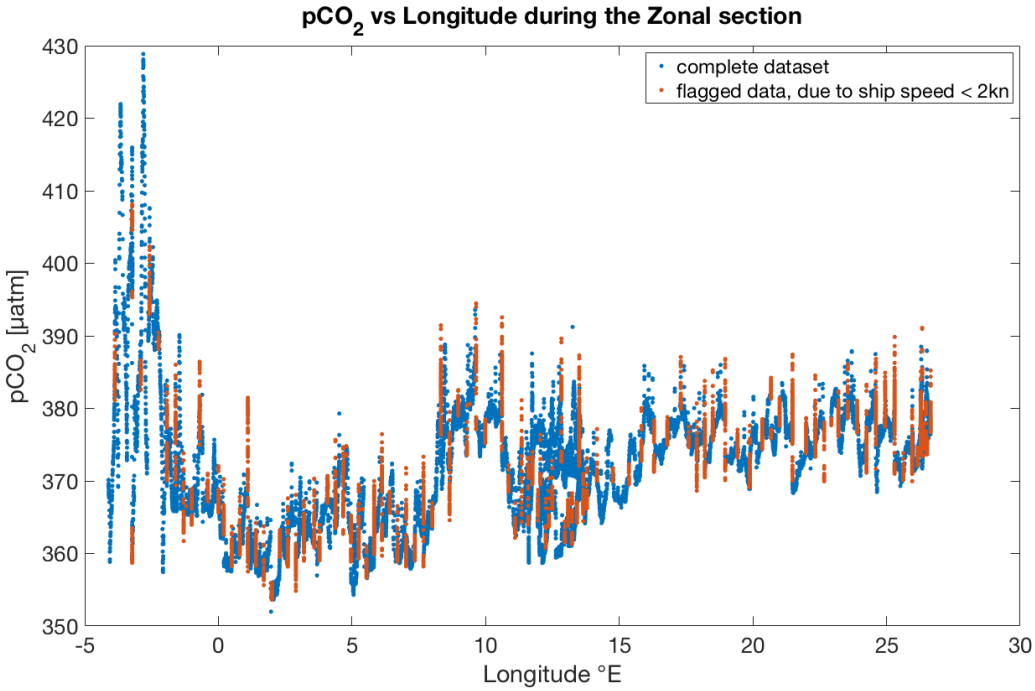

Figure 16: Display of the zonal section plotting pCO_2 vs. longitude and showing the flagged data points where the ship had a speed of <2kn.

(7) In addition, some data points were flagged by hand, when these showed a sudden change in pCO_2 values most likely due to some instrumental problems and uncertainties (see figure 17).

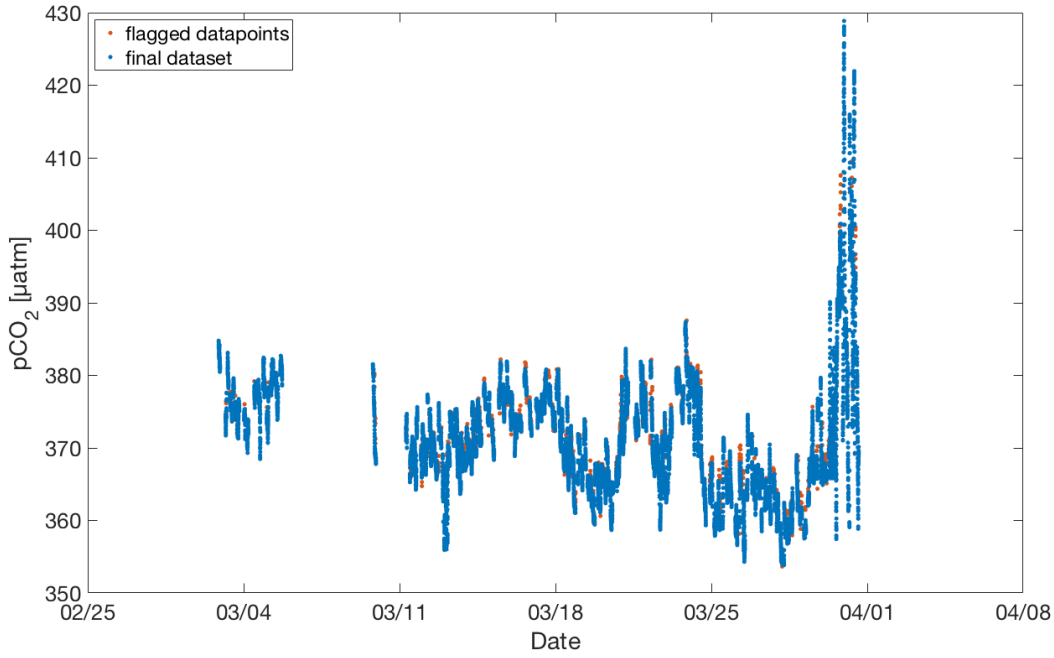

Figure 17: Display of the final flagging (by hand) of data points showing sudden higher or lower pCO_2 values. The blue dots show the final dataset and the red dots mark flagged data points.

The final dataset of measured pCO_2 values obtained after applying these adjustments was used for analysis.

2.2.6 Flagging of the Oxygen-Optode data

Data of the oxygen dataset (see chapter 2.1.5) were flagged by hand to remove sudden increases in the oxygen concentration (see figure 18).

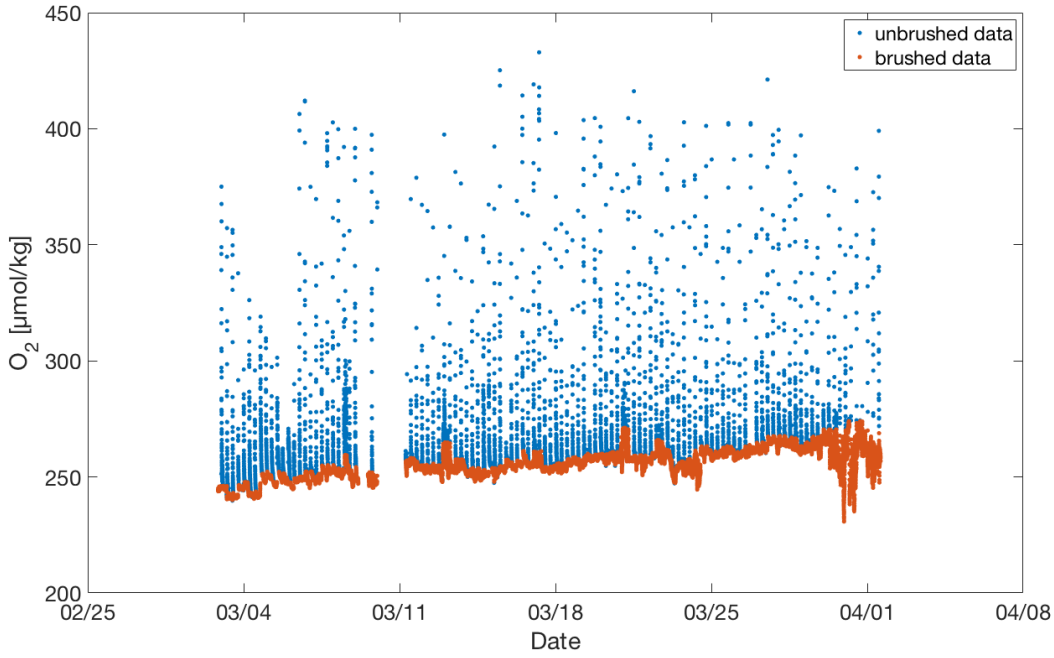

Figure 18: Display of the unbrushed and final brushed data of oxygen concentrations during the cruise MSM 72.

Suddenly increasing oxygen concentrations occurred due to the fact that on the research vessel (Maria S. Merian) two water pump lines alternated in pumping surface seawater into the cooling box. The pumping line, which was not used, was cleaned with a solution and leftovers from this solution caused the aberrantly high oxygen concentrations measured when switching back to this line.

2.2.7 Analysis of the raw oxygen data

Due to the fact that only gas can enter the Optode through the optical isolation layer foil the Optode does not sense any effect of salt and defines oxygen concentrations measured as if in fresh water. Therefore, the influence of salt from the seawater has to be taken into account with help of the following equation.[27]

$$O_{2C} = [O_2] * \exp(S(B_o + B_1 * T_S + B_2 * T_S^2 + B_3 * T_S^3) + C_0 S^2) \quad \textbf{34}$$

with

$[O_2]$ = measured Oxygen concentration

S = measured salinity in ppt

B_0 = -6.24097e^{-3}

B_1 = -6.93498e^{-3}

B_2 = -6.90358e^{-3}

B_3 = -4.29155e^{-3}

C_0 = -3.11680e^{-7}

$$T_S = \ln(\frac{298.15 - t}{273.15 + t})$$

t = measured temperature in °C

2.2.8 Verification of the measured oxygen data

To verify the oxygen data measured with the Optode, some discrete surface samples were taken at specific times during the cruise and the oxygen concentrations were measured manually and compared to the mean of the Optode values from 10 minutes before and after these specific times. The results showed that oxygen concentrations measured in the discrete samples were by a mean of approximately 36.651 µmol/kg higher than those measured in the Optode (see figure 19).

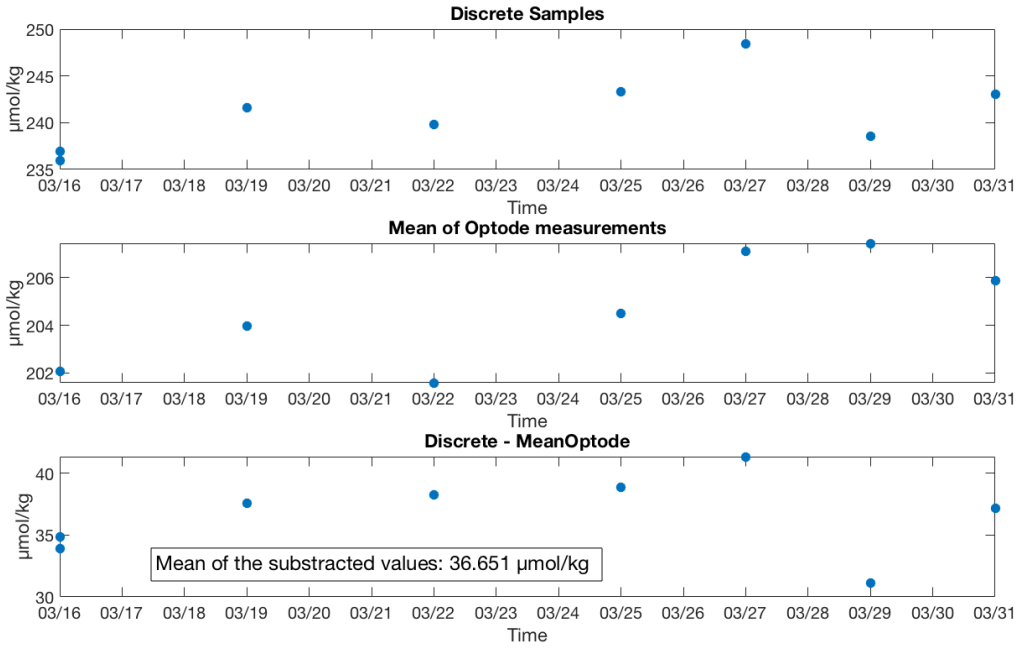

Figure 19: Comparison of the oxygen measurements. Discrete measurements of surface oxygen at specific times during the cruise are shown in the top subplot. The middle subplot shows the mean of the Optode measurements from 10 minutes before and after the specific times of the discrete measurements. The bottom subplot displays the difference between the discrete and the sensor data points and gives the calculated mean.

This difference of 36.651 µmol/kg was therefore added to all data measured with the Optode and yielded a final dataset, which showed good agreement with the discrete measurements (see figure 20).

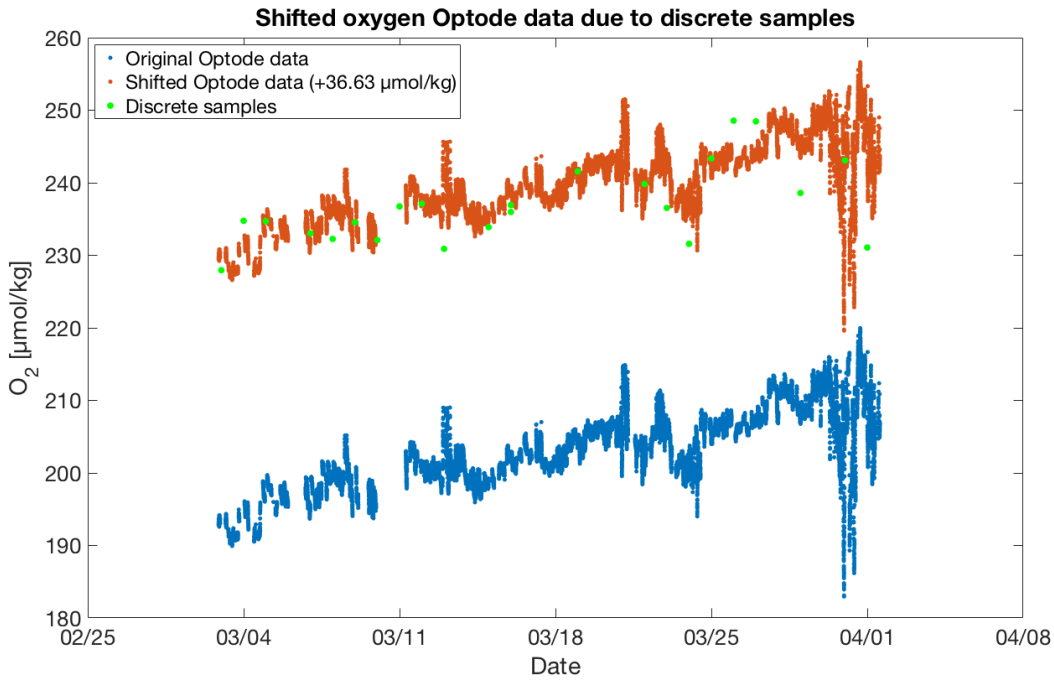

Figure 20: Display of the original dataset of the oxygen values obtained in the sensor in blue, the shifted dataset in orange and some discrete surface measurements shown as green dots.

2.2.9 Atmospheric pCO_2 data

The data for atmospheric CO_2 concentrations were taken from the atmospheric measuring station located on Lampedusa (GLOBALVIEW-CO2, 2018).[37] This station captured data of atmospheric CO_2 [ppm] from 2007 until now (see figure 21).

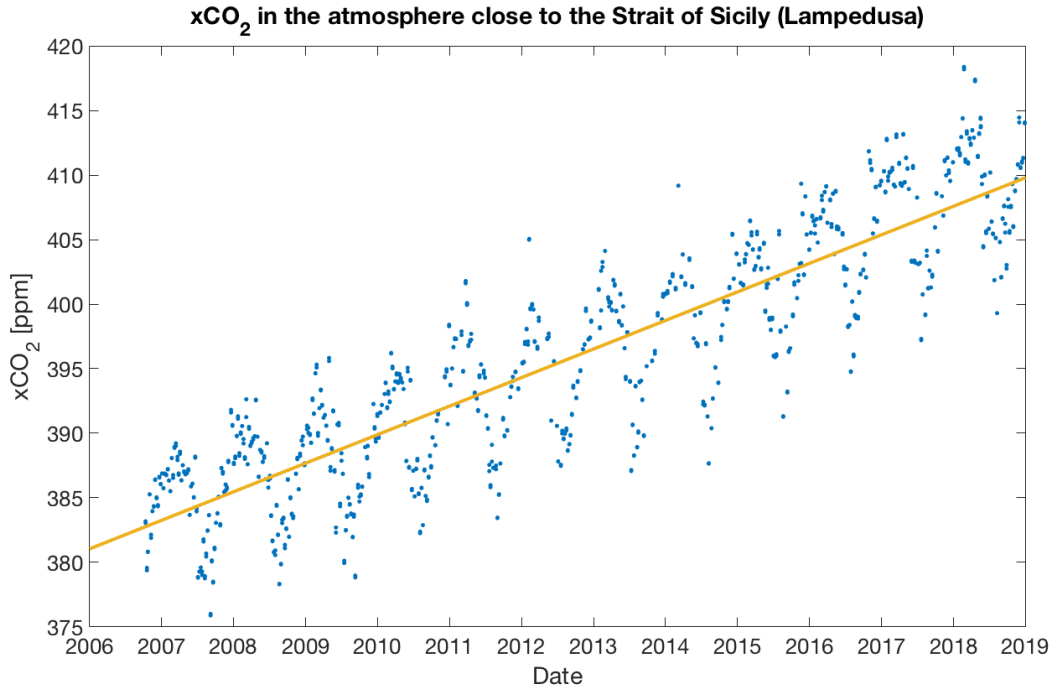

Figure 21: Measured xCO_2 values at the station located on Lampedusa from 2007 till 2019. The linear regression reveals the mean increase of xCO_2 over the years (≈ 2.2 ppm).

The measured concentration on March 16th, 2018 (410.99 ppm) was used for further studies, assuming that this was the xCO_2 (mole fraction of CO_2) in the atmosphere over the entire Mediterranean Sea. Following calculation of pCO_2 via equation 3, the values were used and compared to the measured pCO_2 values of the sensor.

3. Results and Discussion

The partial pressure of CO_2 was measured in two sections of the Mediterranean Sea that were covered during the cruise MSM 72. On one hand, a zonal section starting in Crete and continuing westward through the Strait of Sicily to the Strait of Gibraltar; on the other hand an Ionian section, from Crete through the Ionian Sea to the Otranto Channel along the Greek coast (see figure 22). Below, the results obtained in those two sections will be presented and discussed separately.

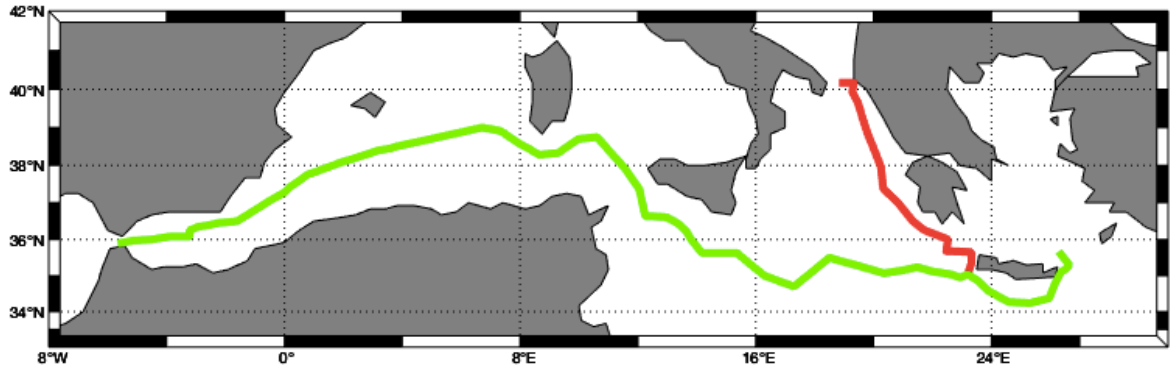

Figure 22: Course of the cruise MSM 72. The green line shows the zonal and the red line the Ionian section.

3.1 Ionian section

Along the Ionian section, pCO_2 data were recorded almost continuously between a latitude of 35 °N and 40 °N. Measurements were carried out twice, on the way north and the way south (see figure 23).

The pCO_2 values obtained showed a relatively constant partial pressure of approximately 370 µatm with variations of ± 5 µatm. Only at the Otranto Strait (40 °N), separating the Ionian Sea from the Adriatic Sea, the values dropped to 355 to 360 µatm.

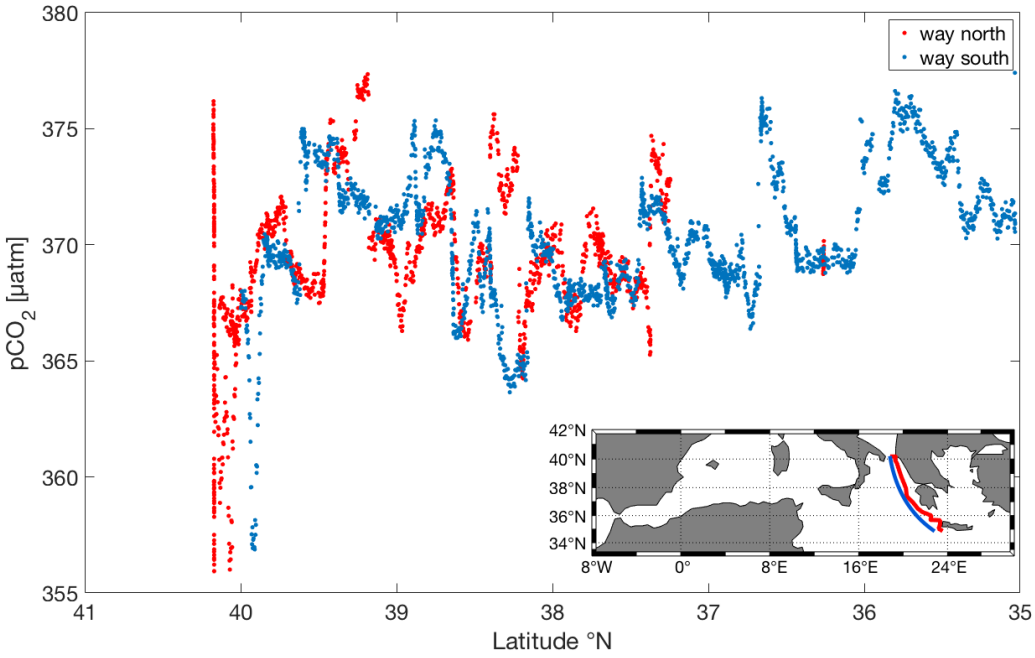

Figure 23: Measured pCO_2 values along the Ionian section plotted against the latitude. The red dots show data obtained while travelling north and the blue while travelling south. Here and in later figures the respective sections analyzed are highlighted in the geographic map.

The data collected during the north- and southbound legs agreed well within ±5 µatm indicating that the sensor worked reliably (measurements were carried out within 10 days and no big variations of pCO_2 are expected to occur during this short period of time).

Next, the influence of temperature and non-temperature dependent effects on pCO_2 along the Ionian section was calculated using the empirical equations of Takahashi et al. (2002):[38]

$$pCO_2(temperature) = mean\ pCO_2 * exp(0.0423 * (observed\ SST - mean\ SST)) \quad \mathbf{35}$$

$$pCO_2(non-temperature) = measured\ pCO_2 * exp(0.0423 * (mean\ SST - observed\ SST)) \quad \mathbf{36}$$

A general temperature influence (pCO_2 (temperature)) is calculated by using a mean value of the pCO_2 over the entire section (mean pCO_2) and the actual sea surface temperature measured at each data point (observed SST), whereas the non-temperature effect (pCO_2 (non-temperature)) considers a mean sea surface temperature over the

entire section (mean SST) and the pCO_2 measured at each data point (measured pCO_2). pCO_2 (temperature) thus specifies pCO_2 values that would have been obtained if only thermodynamic effects of temperature would have had an influence. pCO_2 (non-temperature), on the other hand, depicts the pCO_2 values that would have been obtained if temperature had no influence at all. In the latter case, only factors like currents, upwelling water masses, primary production or consumption and others would have affected the pCO_2.

A comparison of the calculated pCO_2 (temperature) and pCO_2 (non-temperature) data with the measured pCO_2 values along the Ionian section is depicted in figure 24. The green line shows the pCO_2 if only temperature would affect its value during this specific section and the red line if temperature would have no influence at all. Variations are highest in the Strait of Otranto, where both effects appear to have an influence on the measured pCO_2. However, as the measured data were closer to those calculated with temperature influence it appears that temperature effects were dominant in affecting the pCO_2 at this point. Non-temperature effects, such as biological production or consumption of CO_2, lateral and vertical mixing, salinity differences and pressure changes, appeared to only have a smaller effect. Thus, the sudden decrease of temperature in the Otranto Strait was most likely the main cause for the observed decrease in pCO_2 values at this latitude.

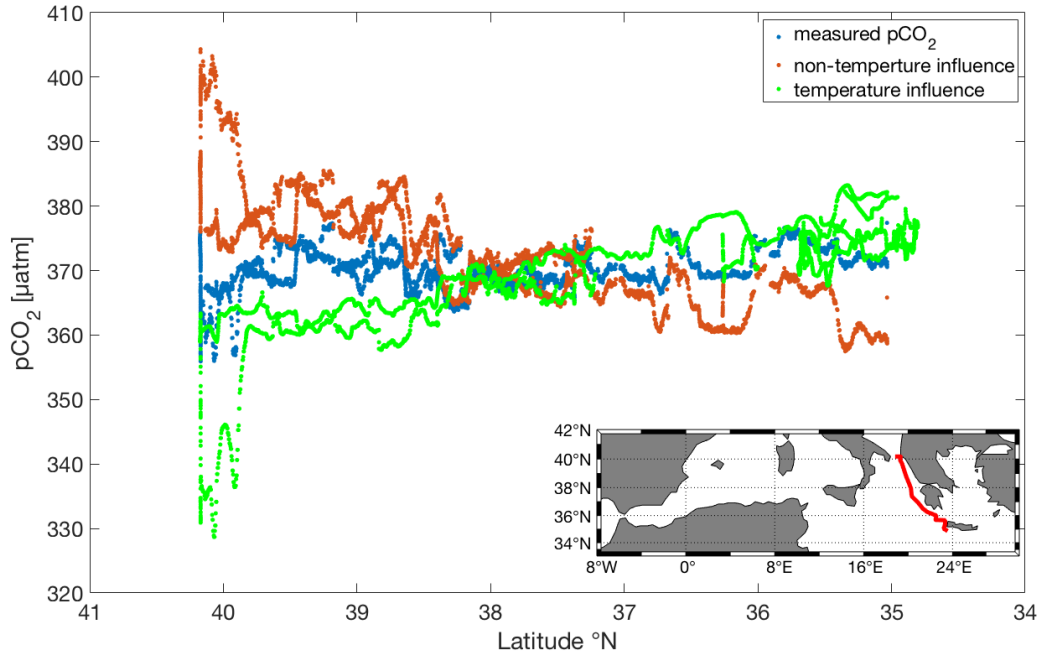

Figure 24: Temperature and non-temperature dependent effects on pCO_2. The values were plotted against the latitude in the Ionian section. The blue data show the measured pCO_2 values, the green data are the calculated pCO_2 values when only a temperature influence is considered and the red show pCO_2 values calculated with a mean temperature of the entire section, i.e. when a specific temperature influence is not considered.

Next, a potential effect of certain currents on the pCO_2 distribution was analyzed more closely by inspecting satellite maps of the region. However, as shown in figure 25, no specific currents were visible in the satellite image of the Ionian section in the Otranto Strait taken at the time of the pCO_2 recordings.

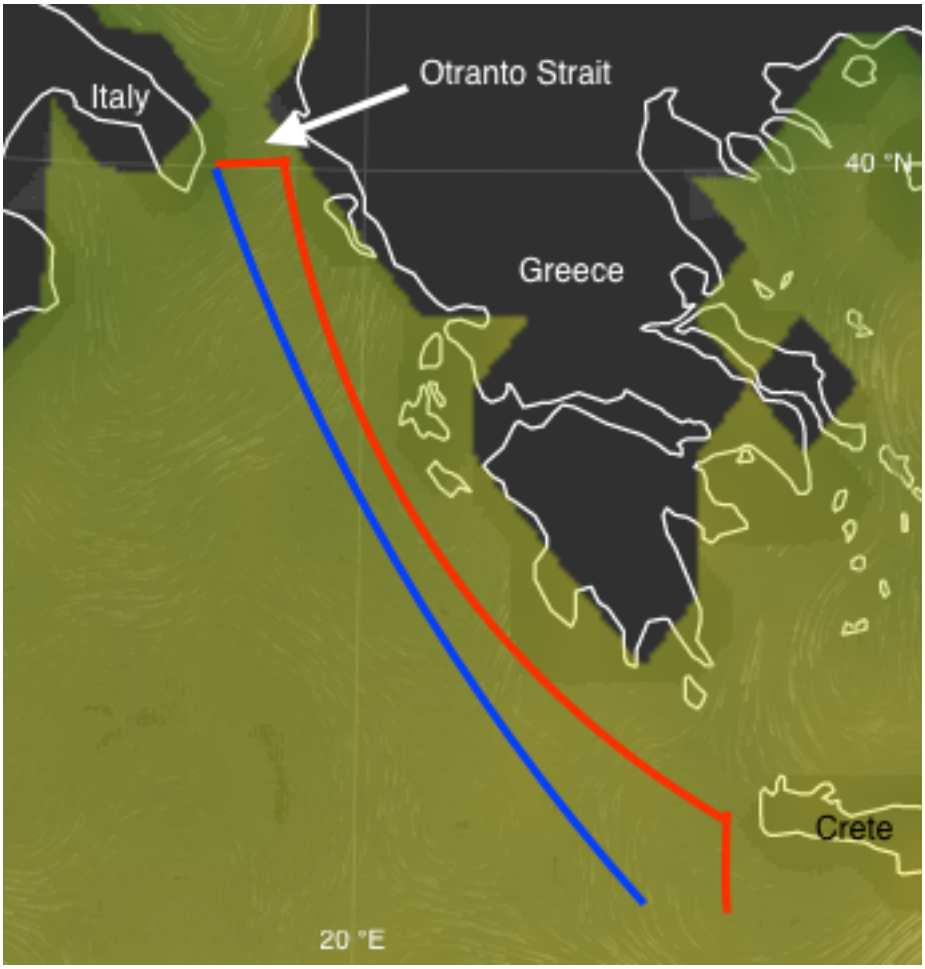

Figure 25: Satellite image of currents occurring in the area of the Ionian section at the time of the cruise (10th of March 2018) taken from https://earth.nullschool.net.[39] The red line shows the route of the cruise on the way north and the blue line on the way south.

This suggests that the non-temperature influence, which would cause higher pCO_2 values at a latitude of around 40 °N, is probably not caused by certain currents but rather by vertical mixing, most likely as a result of the upwelling of water masses (LIW) with higher pCO_2 in the shallow Strait.

Phototrophic bacteria and algae performing photosynthesis and thus consuming CO_2 and, on the other hand, CO_2 producing organisms in the water could possibly cause the variations of ± 5 µatm seen in the measured data and the periodically occurring higher and lower pCO_2 values. At night, no photosynthesis can be performed and no CO_2 is transformed into oxygen, whereas during the day these processes would lead to lower values of pCO_2. To test this hypothesis, differences between the day and night measurements during the Ionian section of the cruise were inspected. Figure 26 reveals that similar variations were observed during day and night, suggesting that they were not caused by photosynthetic activity. Day hours were set to 5 am till 5 pm UTC

(Coordinated Universal Time) based on the sunrise and sunset on Crete in the beginning of March.

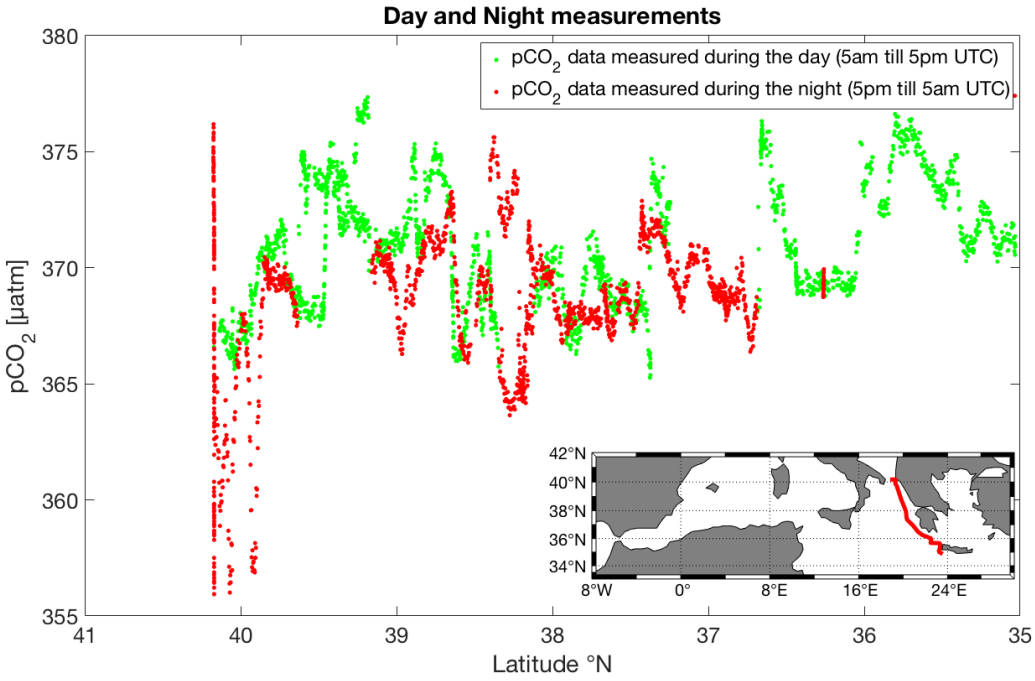

Figure 26: Measured pCO_2 values during the Ionian section plotted against the latitude. The red dots show data obtained during night measurements and the green during day measurements.

Thus, the rather minor variations of 5 µatm were most likely caused by small temperature changes and small variation in the water masses occurring due to currents. As seen in figure 25, with the exception of the Otranto Strait, currents were visible over almost the entire section.

3.2 Zonal section

The final, flagged and processed pCO_2 data for the zonal section are shown in figure 27. The recordings covered a longitudinal path from the east of Crete at a longitude of 26.5 °E to the Strait of Gibraltar at a longitude of 5 °W with a short path into the Tyrrhenian Sea at a longitude of 12 °E.

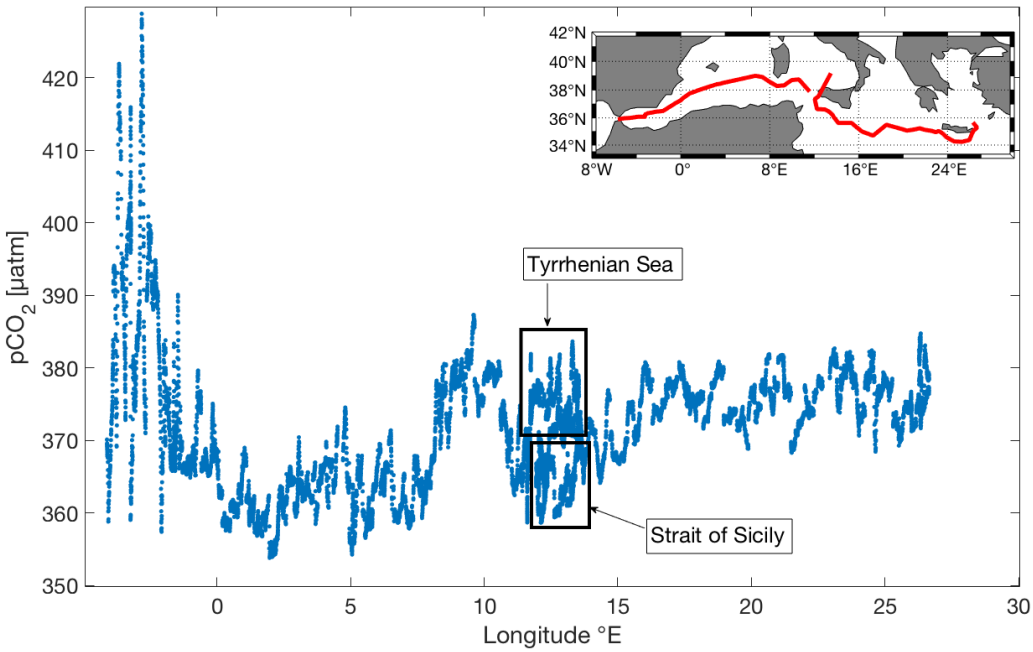

Figure 27: Display of the zonal section pCO_2 values plotted against the longitude. Recordings in the Strait of Sicily and the Tyrrhenian Sea are shown in parallel because the cruise first sailed north into the Tyrrhenian Sea from the Strait of Sicily at a latitudinal section before continuing along the zonal section.

Figure 27 shows that the pCO_2 values of the surface water were approximately 10 µatm higher in the Eastern Mediterranean basin (375 µatm), i.e. at longitudes between 15 °E and 26 °E, as compared to the Western Mediterranean basin (365 µatm) located at longitudes between 0 °E and 8 °E. This difference could be due to the fact that the Atlantic Water (AW), which accounts for the surface water, moves from west to east in the Mediterranean Sea and during this movement has the opportunity to exchange CO_2 with the atmosphere via air-sea gas exchange. This will lead to higher pCO_2 values the further east the surface water is analyzed. Moreover, as reported by Powley et al. (2017) the primary production in the Western Mediterranean Sea (WMS) is 2.5 to 3.3 times higher than in the Eastern Mediterranean Sea (EMS), resulting in higher pCO_2 in the eastern basin.[40] Another reason could be colder sea surface temperatures measured in the WMS compared to the EMS.

The pCO_2 in the atmosphere measured at Lampedusa in mid-March 2018 showed values of around 410 ppm. As these values were generally higher than those obtained for the surface water during the cruise, a net influx of CO_2 from the atmosphere could be expected over almost the entire Mediterranean Sea. This contrasts measurements carried out in October/November of 2001, when a flux of CO_2 from the Sea to the

atmosphere had been considered.[41] The pCO_2 values in this earlier study were calculated from DIC and TA measurements and revealed values of around 400 µatm inside the Med with the atmosphere containing approximately 375 ppm. The net uptake of CO_2 from the atmosphere resulting in high surface water pCO_2 was discussed to have resulted from fast deep water formation and a low Revelle factor within the surface water due to higher SST.[41] Major differences between the 2001 measurements and the ones carried out during MSM 72 in 2018 are the different times of the year (March vs. October/November) and the detection methods (calculations from DIC and Alkalinity vs. direct underway measurements). Both factors could represent a cause for the different seawater to atmospheric CO_2 ratio estimations, one showing an undersaturation of the seawater (measurements during MSM 72) and the other an oversaturation with CO_2 (measurements from 2001).[40,41]

Influx and efflux of CO_2 in the Med were also compared by inspecting the general differences in fugacity (ΔfCO_2) during a year. This revealed that during the winter months (November till Mai) a net CO_2 influx from the atmosphere is expected, whereas during the summer months (May till November) a net efflux of CO_2 to the atmosphere is observed (see figure 28). The ΔfCO_2 is used to indicate if fCO_2 in the atmosphere is higher or lower compared to that in the surface water at the respective time of year. This comparison will not consider that CO_2 in the atmosphere and seawater has increased over the years, but will only monitor a time-independent flux. In this comparison, values above 0 indicate that the seawater fCO_2 was higher compared to the atmospheric fCO_2 and values below 0 show the opposite.

CO_2 measurements that were carried out in the Mediterranean Sea during a time period from 1995 till 2018 were taken into account (SOCAT) and the fugacity of CO_2 measured in the atmosphere of each specific year (taken from the Lampedusa data) was subtracted from the seawater fCO_2 measured in the respective year. As the SOCAT data only contained fugacity values (fCO_2), the atmospheric concentration of CO_2 and the measured pCO_2 during cruise MSM 72 were transformed into fCO_2 via equations 29 and 30 (see chapter 2.2.1). However, because the differences between the partial pressure and the fugacity of CO_2 are only minor, the analysis of the cruise data was further on continued with the measured pCO_2 values.[37,42]

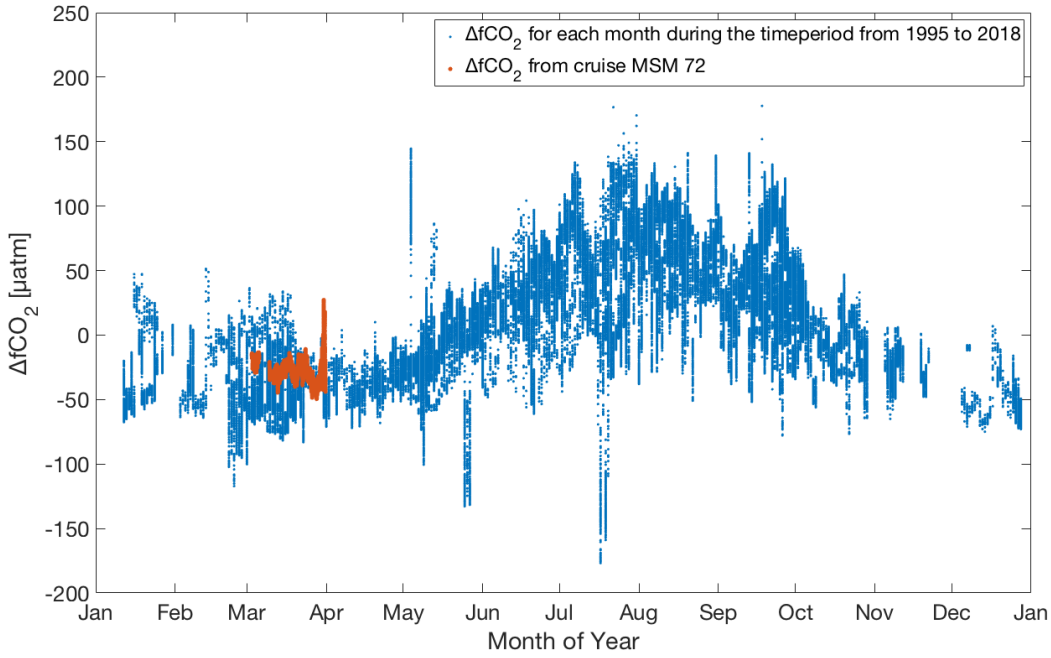

Figure 28: Display of the ΔfCO_2 during one year inside the Mediterranean Sea. Blue data represent the measurements for years 1995-2018 taken from SOCAT. They are compared to data obtained during the cruise MSM 72 (shown in red). Negative ΔfCO_2 values indicate undersaturation of the seawater and thus the occurrence of net influx, whereas positive values indicate efflux from the water into the atmosphere.

Figure 28 shows that the data measured during cruise MSM 72 match the general pattern of ΔfCO_2 in the Mediterranean Sea during March, i.e. a general undersaturation during this time of year.

While pCO_2 values in surface waters of the zonal section dropped to 365 µatm at the Strait of Sicily, they increased within the Tyrrhenian Sea (375 µatm) and further in the Sardinia Channel at a longitude of 8-10 °E (380 µatm) (see figure 27). The shallow Sardinia Channel, where Levantine Intermediate Water (LIW) is upwelling and mixing with the TDW (Tyrrhenian Deep Water), could cause these higher pCO_2 values in the surface water. The Mixed Layer Depth (MLD) at the Sardinia Channel was at a depth of approximately 100 m during the time of the cruise (see figure 29) and therefore a mixing of AW with upwelling LIW at 100 m depth could affect surface water values of pCO_2. The MLD describes the depth until the temperature of the surface water has decreased by more than 0.5 °C or, as used throughout this thesis, until the oxygen concentration has decreased significantly.[43] In fact, the shallowest part of the Sardinia Channel is also only 100 m deep enforcing a mixing of upwelling LIW, which moves westward, with the eastbound moving AW. As reported by Anderson and Olsen (2002),

this vertical mixing affects the increase of pCO_2 in the surface water and is of significant importance. The MLD generally increases inside the Med from November to March and reaches its maximum value between February and March (Miquel et al., 2011), before decreasing to a minimal value of 30 m during the summer due to stratification (Nykjaer, 2009).[44,45,46]

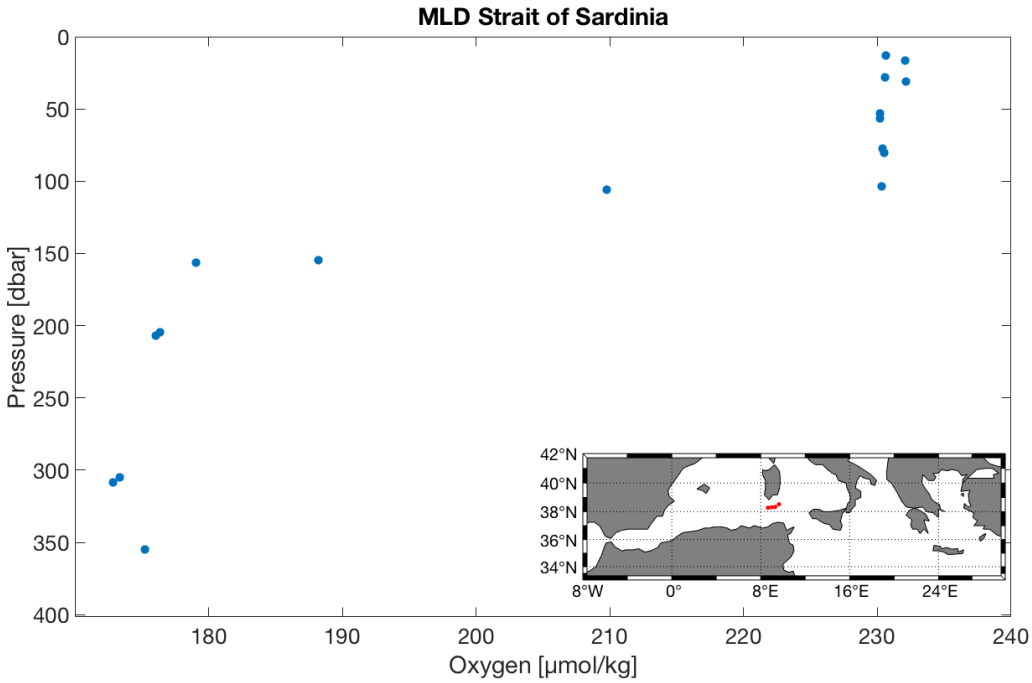

Figure 29: Depth profile of dissolved oxygen at stations 87 till 90. The sharp oxycline at 100 to 150 m depth denotes the MLD.

Upon entering the Western Mediterranean basin west of the Strait of Sardinia, the partial pressure of surface water CO_2 dropped suddenly and then stayed at around 365 ± 7 µatm (see figure 27).

Further west, close to the Strait of Gibraltar (-3 °E) in the Alboran Sea, the pCO_2 values showed high variations ranging from 360 to 430 µatm. How could these variations be explained? Upwelling LIW again could cause increased surface pCO_2 at these longitudes as LIW carries water with higher pCO_2 as compared to surface water (AW). Higher pCO_2 values inside the LIW are typically caused by respiration and are also due to the already higher pCO_2 values in the surface waters of the EMS that sink to form the LIW in the Levantine basin. Moreover, a small branch of the AW, which had traveled from the north end of the Tyrrhenian Sea through the Balearic Sea back to the Strait of Gibraltar, mixes in the Alboran Sea with the AW flowing in from the Atlantic. This water mass should also

show higher pCO_2 values due to the fact that more air-sea gas exchange occurred during its movement through the Western Med and Tyrrhenian Sea. It should also be noted that the coastal regions are very close to the cruise track before and in the Strait of Gibraltar and these regions are usually characterized by higher pCO_2 values as compared to the open sea due to factors such as freshwater input, coastal upwelling and biological activity.[47]

The high variations occurring close to the Strait of Gibraltar could also be caused by temperature changes, in particular in shallow coastal regions, as well as currents or eddies occurring in these parts. These factors are discussed in more detail below where different parts of the zonal section are presented (see chapter 3.3).

In contrast to the Straits of Sardinia and Gibraltar, the level of pCO_2 inside the Eastern and Western Mediterranean basin remain relatively constant. This is most likely due to the fact that in the open sea variations based on vertical mixing, algal blooms or rapid growth of other organisms are less likely to occur.

3.3 Separated zonal sections

In the following, the zonal section was divided into four different parts (Eastern Mediterranean basin, Tyrrhenian Sea, Western Mediterranean basin and the Alboran Sea), which were characterized in more detail. A first comparison of the three subsections and the separately treated Ionian section used the Temperature-Salinity-Diagram, which revealed different temperature-salinity-anomalies (see figure 30).

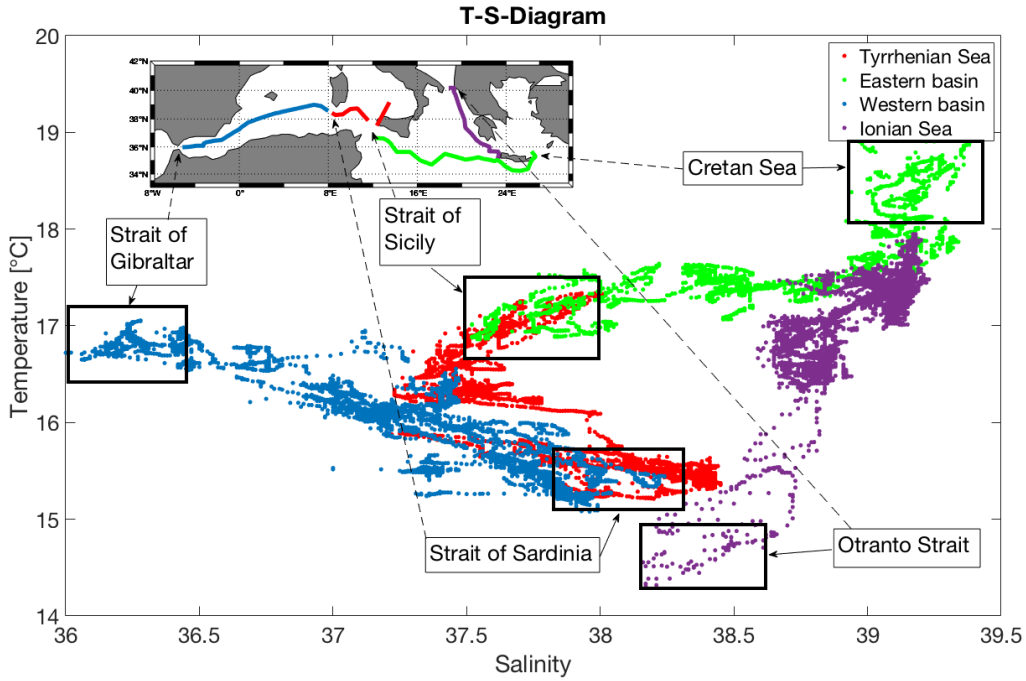

Figure 30: Temperature-Salinity plot of different sections of the cruise. The Western Med is displayed in blue, the Tyrrhenian Sea in red, the Eastern Med in green and the Ionian section in purple.

The figure clearly shows that the salinity of the surface water increased from the Strait of Gibraltar in the west towards Crete as the most eastern part. This is mainly due to evaporation of the AW. The T-S plot also reveals that the average temperature was approx. 1.5 °C lower in the Western Med compared to the Eastern, which might have caused the slightly lower pCO_2 values in the Western Med. Interestingly, in most of the Tyrrhenian Sea, the salinity decreased slightly and the temperature increased as compared to the Sardinia Channel. This is probably due to different upwelling and mixing water masses, currents and Eddies present in this part of the Mediterranean Sea. Entering the Eastern Med, the temperature stayed rather constant and the salinity increased until east of Crete, where the temperature suddenly rose by 1 °C. This increase is most likely caused by the Cretan Surface Water (CSW), which mixes with the eastbound moving AW at this point. Figure 30 also shows that the salinity stayed rather constant in the Ionian section indicating that less evaporation occurred here. Moreover, a temperature decrease of 2 °C from 16.5 °C to 14.5 °C was observed in this section, in particular close to the Strait of Otranto in the northern part of the Ionian section. This correlates with reduced pCO_2 values in this part as described in chapter 3.1.

3.3.1 Eastern Mediterranean basin

Figure 31 reveals a more detailed presentation of the pCO_2 values measured in the eastern basin of the Mediterranean Sea. Here the cruise covered a section from the east of Crete at a longitude of 26.5 °E to the Strait of Sicily at a longitude of 12 °E and a latitude range from 34.2 °N to 36.6 °N.

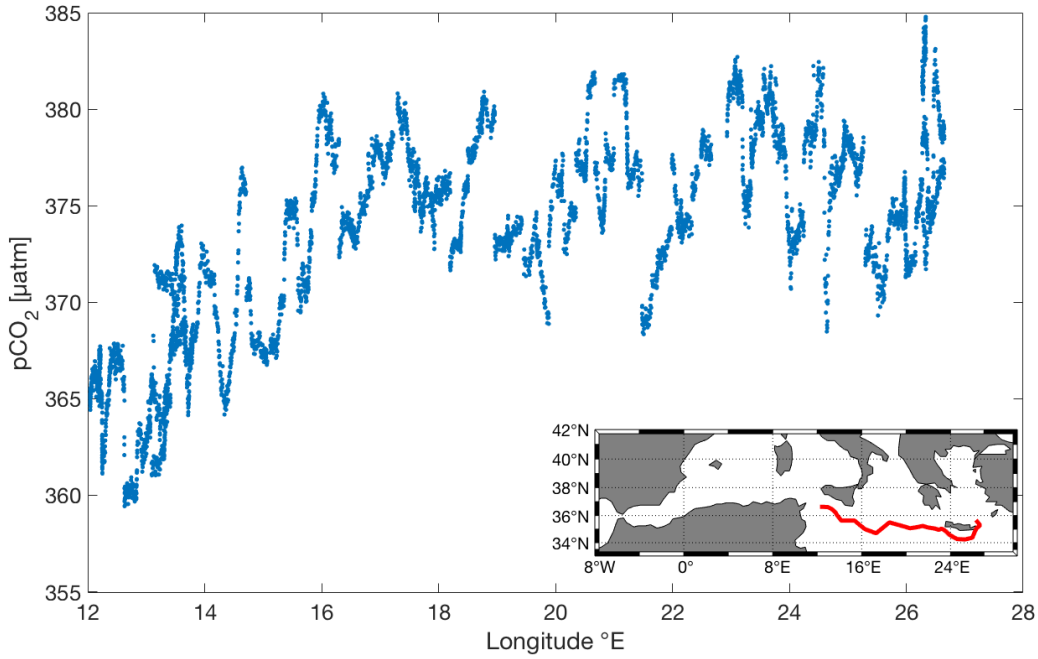

Figure 31: Measured pCO_2 in the eastern basin of the Mediterranean Sea plotted against the longitude.

It is evident that the partial pressure of CO_2 remained relatively constant in the eastern basin. With variations of ±5 µatm a mean value of 375 µatm was observed. The small variations are most likely due to small temperature changes and smaller currents occurring along the cruise. As already described in chapter 3.1 and also shown in figure 32 they were not caused by day/night variations reflecting different photosynthetic activities.

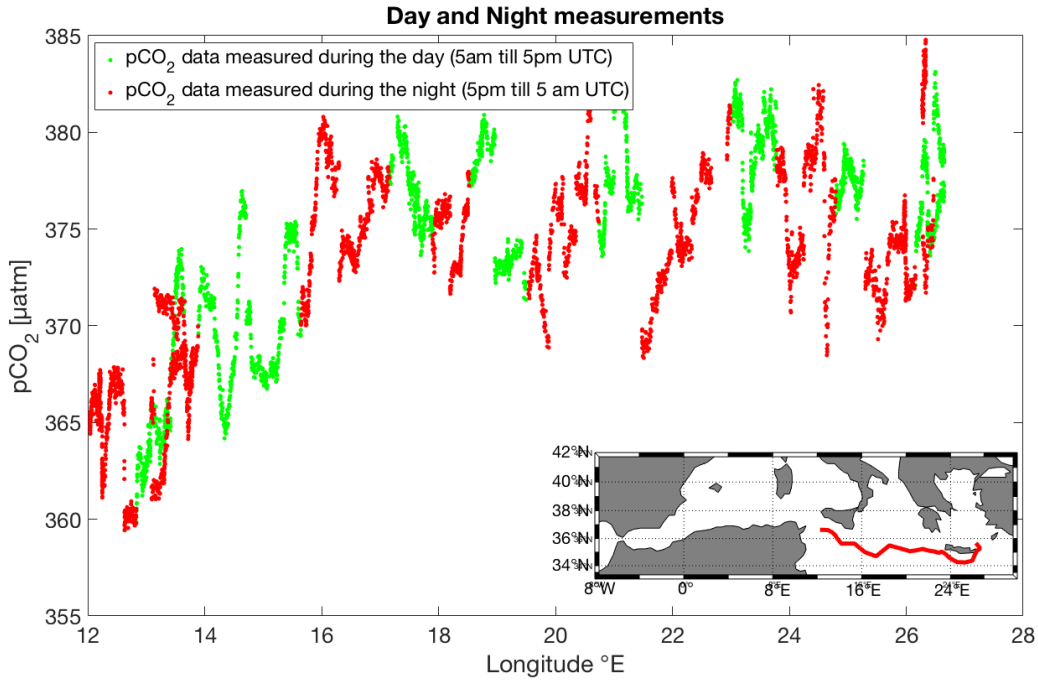

Figure 32: Measured pCO_2 values in the eastern basin plotted against the longitude. The red dots show data obtained during night measurements and the green those obtained during day measurements.

Slightly higher pCO_2 values were measured in the northeast of Crete at a longitude of 26.5 °E, where the Cretan Sea borders on the Levantine basin. Most likely, these are caused by a mixing of the Cretan Surface Water (CSW) with the AW. Further west, closer to the Strait of Sicily, pCO_2 values decreased a little to 365 µatm. An inspection of the temperature and non-temperature influences on the pCO_2 values in this region revealed that the pCO_2 decrease is primarily caused by temperature influences at this longitude (see figure 33).

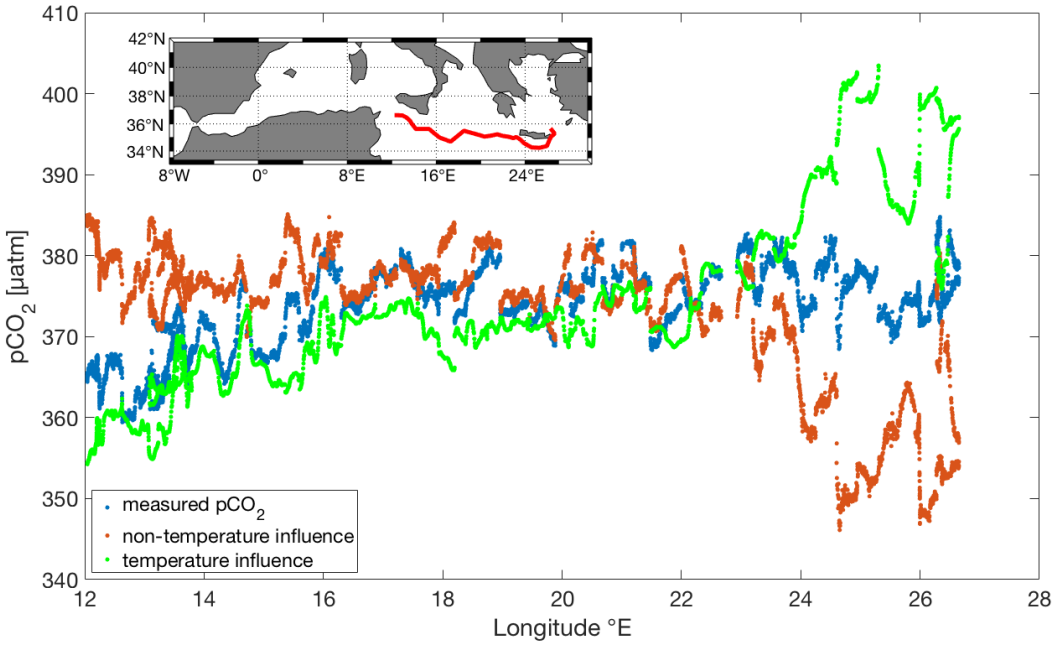

Figure 33: Temperature and non-temperature dependent effects on pCO_2. The values were plotted against the longitude in this eastern part of the zonal section. The blue data show the measured pCO_2 values, the green data are the calculated pCO_2 values when only a temperature influence is considered and the red show pCO_2 values calculated with a mean temperature of the entire section, i.e. when a specific temperature influence is not considered.

However, the plot also shows that non-temperature dependent effects have to be considered as well. For example, close to the Strait of Sicily (12 to 16 °E) these effects slightly dampened the temperature dependent effect on the pCO_2 values and in the far east at the island of Crete the non-temperature influences balanced out the effect of the temperature influences. In fact, at longitudes between 16 and 26 °E the temperature and non-temperature effects canceled out one another and an almost constant pCO_2 of 375 µatm was observed.

What could be the reason for the substantial non-temperature effects at longitudes between 24 °E and 26.5 °E? In the northeast of Crete at a longitude of 26.5 °E, where the cruise started and higher pCO_2 was detected, the CSW might have mixed with the AW as described above. As compared to the incoming AW, the CSW had more time to equilibrate with the atmospheric CO_2 resulting in slightly higher pCO_2 values. In contrast, non-temperature effects in the south of Crete, between a longitude of 24 °E and 26 °E, would cause a clear decrease of pCO_2 if no temperature-dependent increase would counteract this. This is probably due to an anticyclonic current (Eddy), which was observed at these longitudes during the time the cruise passed (see figure 34), and most

likely caused a vertical mixing of water masses. Possibly a smaller algal bloom consuming CO_2 also occurred shortly before or at the time of the cruise in the south of Crete. Another possibility resulting in lower pCO_2 values could be that the Eddy carried the results of an algal bloom (lower pCO_2 and higher O_2 values) or even the algae themselves from somewhere else in the Mediterranean Sea.

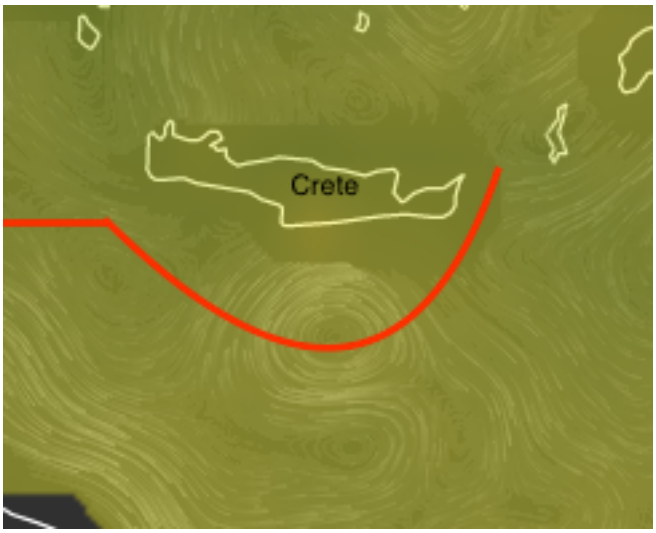

Figure 34: Satellite picture of currents occurring in the south of Crete at the time of the cruise (4th of March 2018) taken from https://earth.nullschool.net.[39] The cruise track is displayed as a red line.

Such interpretation is also in line with the oxygen saturation calculated from the measured oxygen concentrations during the cruise revealing differences from oxygen being in equilibrium with the atmosphere ($\Delta O_2 = 0$) (see figure 35). At a longitude of 24 °E a net increase of oxygen was apparent, which could have resulted from an algal bloom producing oxygen (and consuming CO_2) through photosynthesis.

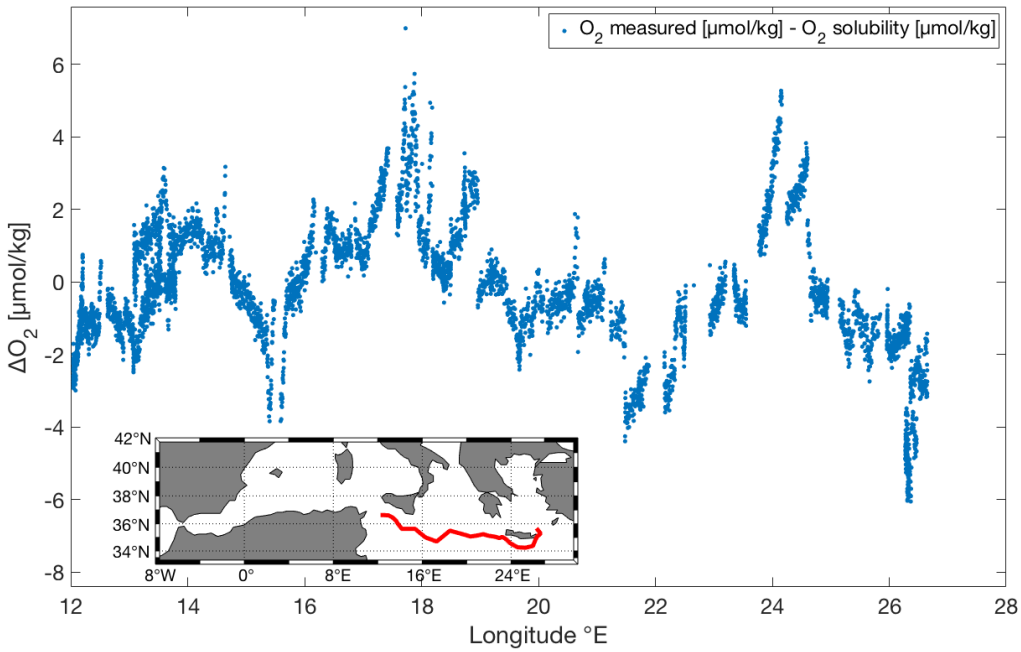

Figure 35: Oxygen saturation calculated from measured oxygen minus oxygen solubility inside the Eastern Mediterranean basin displayed in µmol/kg and plotted against the longitude.

The oxygen saturation plot also reveals that in the north-east of Crete, at a longitude of 26.5 °E, oxygen is consumed, most likely resulting in a production of CO_2 seen as higher pCO_2 values in figures 31 to 33.

As the temperature (see figure 30) and pCO_2 (see figure 31) remained relatively constant within most parts of the eastern basin but the salinity increased (see figure 30), salinity only appeared to have a minor or even negligible influence on the partial pressure of CO_2. Moreover, as discussed above the influences of temperature and non-temperature effects are either very minor or level out each other at these longitudes (16-24 °E). Thus, in the open ocean of this part of the Med the partial pressure of CO_2 was mainly influenced by air-sea gas exchange and thereby remained at a relatively constant level.

3.3.2 Tyrrhenian basin

After passing the Strait of Sicily the cruise MSM 72 entered the Tyrrhenian Sea and then first covered a latitudinal section into the middle of the Tyrrhenian Sea, before continuing the zonal section. The pCO_2 measured along the latitudinal section is shown in figure 36 covering a latitude change from 37.9 °N to 39.2 °N.

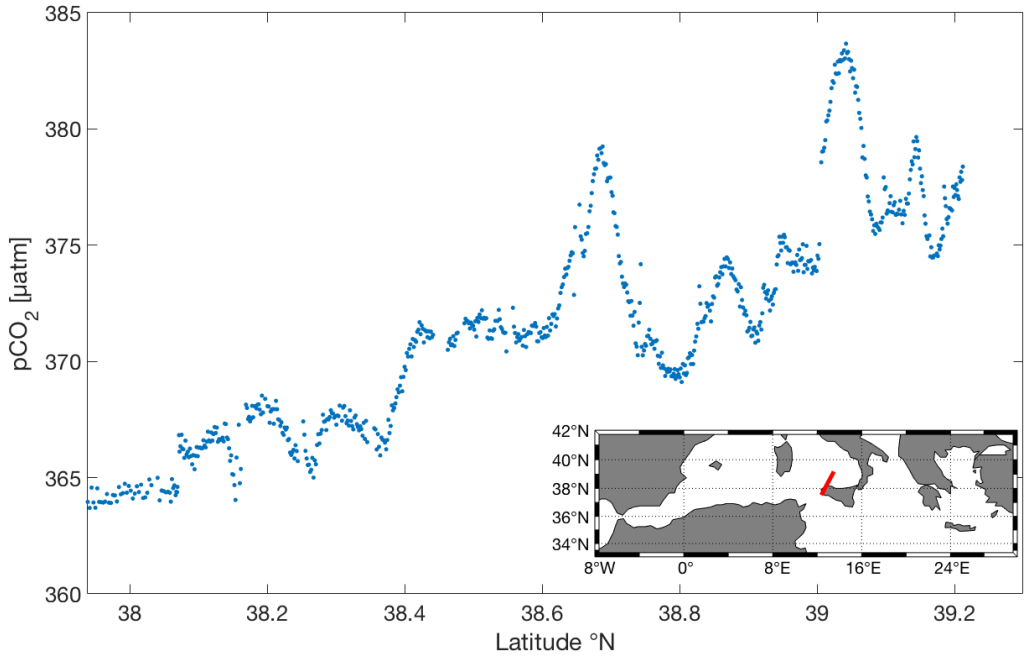

Figure 36: Measured pCO_2 along a latitudinal section of the Tyrrhenian basin plotted against the latitude.

The plot shows that the partial pressure of CO_2 increased with latitude. Most likely, this is either caused by increasing temperatures or by mixing water masses, oxygen consumption and currents or eddies occurring in this area. To differentiate between these effects, the role of temperature versus non-temperature influences was again considered using the empirical equations of Takahashi et al. (2002).[38]

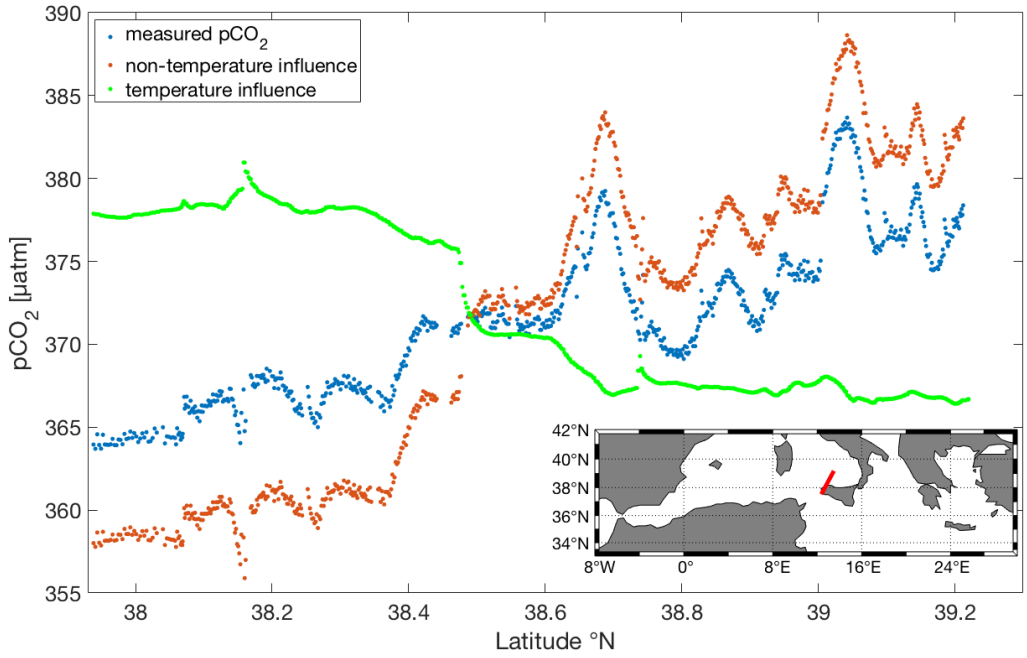

Figure 37: Temperature and non-temperature dependent effects on pCO_2. The values were plotted against the latitude in this section of the Tyrrhenian Sea. The blue data show the measured pCO_2 values, the green data are the calculated pCO_2 values when only a temperature influence is considered and the red show pCO_2 values calculated with a mean temperature of the entire section, i.e. when a specific temperature influence is not considered.

As shown in figure 37 the driving factor for the elevated pCO_2 levels in this part of the Tyrrhenian basin (latitudes 38 °N to 39.2 °N) was mainly non-temperature based. The temperature influence on the pCO_2 measured in this region of the Mediterranean Sea again counteracted non-temperature effects but was less effective. The solely temperature-influenced pCO_2 values decreased at a latitude of 38.45 °N and remained rather constant thereafter. This could indicate that the AW was separated at this point, one branch moving into the Tyrrhenian Sea and the other part flowing into the eastern basin, being affected by upwelling LIW at this latitude (see figure 38).

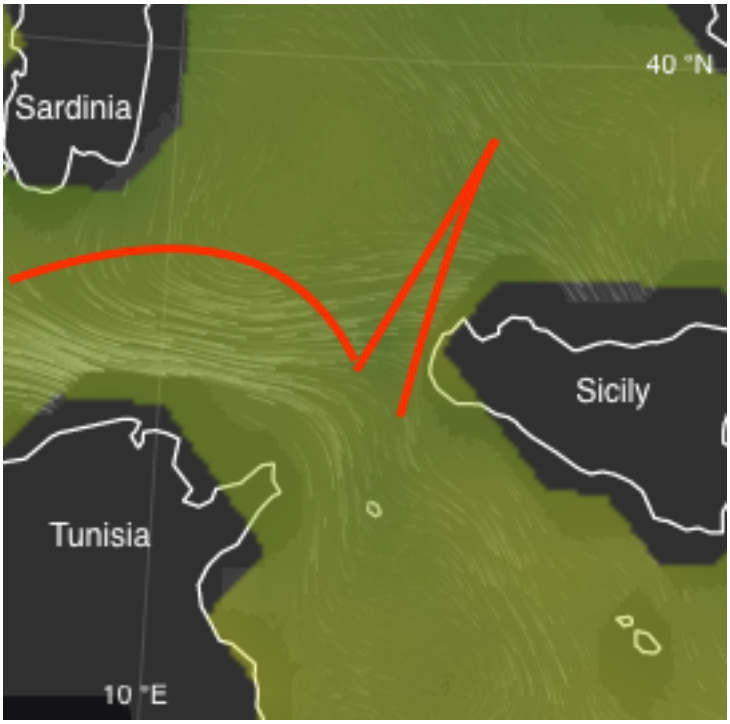

Figure 38: Satellite picture of currents occurring in the Tyrrhenian Sea during the time of the cruise (23rd of March 2018) taken from https://earth.nullschool.net.[39] The route at the cruise through the Tyrrhenian Sea is highlighted with the red line.

The increase in pCO_2 observed along this part of the cruise, i.e. upon moving further north into the open sea is unexpected as the partial pressure of CO_2 usually decreases further away from the coast. This could be due to major consumption of oxygen and an accompanying production of CO_2 in this area or a mixing of deeper water masses occurring at this point. Eddies present at this latitude and longitude could also contribute to the unusual pCO_2 increase. Inside an Eddy, the presence of oxygen consumers could lead to a local increase in pCO_2 that will not easily dissipate by mixing with surrounding water. However, the oxygen saturation plot shown in figure 39 reveals that its consumption along this section of the Tyrrhenian Sea was rather negligible. The saturation values at latitudes between 38.7 and 38.9 even show that oxygen is not consumed but rather formed, which normally would correlate with decreasing pCO_2.

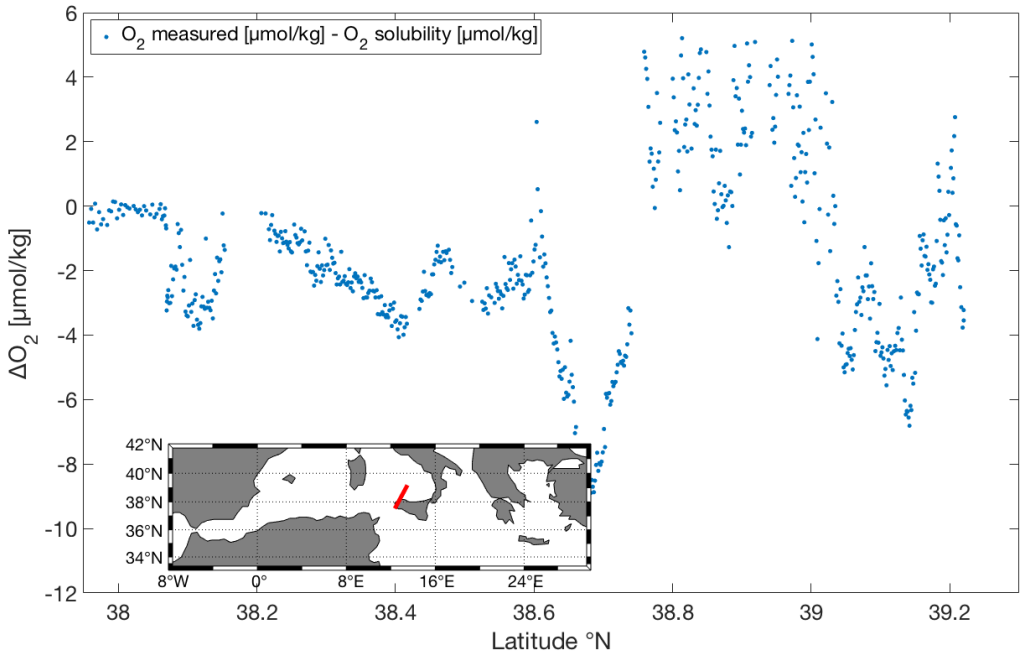

Figure 39: Oxygen saturation calculated from measured oxygen minus oxygen solubility inside the latitudinal section of the Tyrrhenian Sea displayed in µmol/kg and plotted against the longitude.

Only at latitudes between 38.6 °N and 38.7 °N a consumption of oxygen was apparent, which could contribute to the increasing pCO_2 values at these latitudes. Thus, it appears that other non-temperature influences are a major cause of the increased pCO_2 measured in this part of the Tyrrhenian basin. These could include a vertical mixing of water masses as a result of upwelling possibly caused by currents and water movement inside the Tyrrhenian Sea as shown in the Satellite picture (see figure 38).

The pCO_2 values measured during the second part of the cruise through the Tyrrhenian basin, now along the zonal section, are displayed in figure 40.

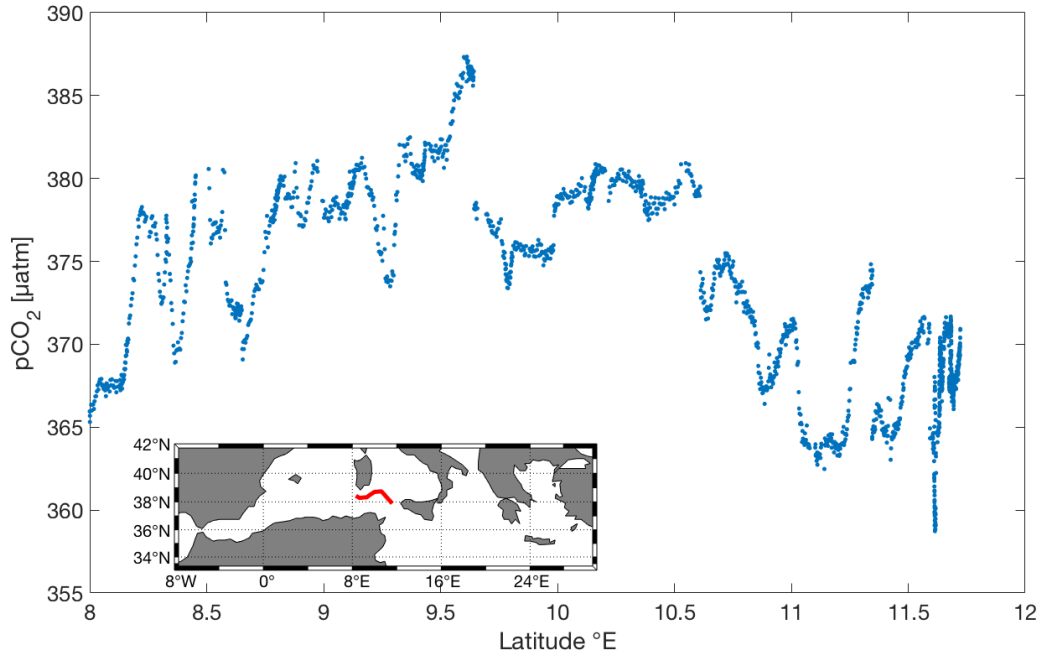

Figure 40: Measured pCO_2 in the second, zonal part of the cruise through the Tyrrhenian basin plotted against the longitude.

The partial pressure of CO_2 showed lower values of 365 to 370 µatm between longitudes 11 °E and 12 °E but values slightly increased further west, i.e. closer to the Strait of Sardinia. West of a longitude of 10.4 °E, the pCO_2 was relatively constant at 375 µatm with variations of ±5 µatm. Only at the far western end of this section (8 °E), while entering the western basin of the Med, the values dropped again to 365 µatm.

The higher values close to and inside the Sardinia Channel (longitudes 8.5 °E to 10.5 °E) could be caused by LIW upwelling that occurs at these longitudes during LIW movement towards the Atlantic Ocean, as discussed in chapter 3.2. This would be considered a non-temperature related effect and figure 41 shows that such effects were the driving factor for the increased pCO_2 values in this zonal section of the Tyrrhenian Sea. As the temperature influence stayed relatively constant along the entire section, significant changes in the pCO_2 values would require a non-temperature influence.

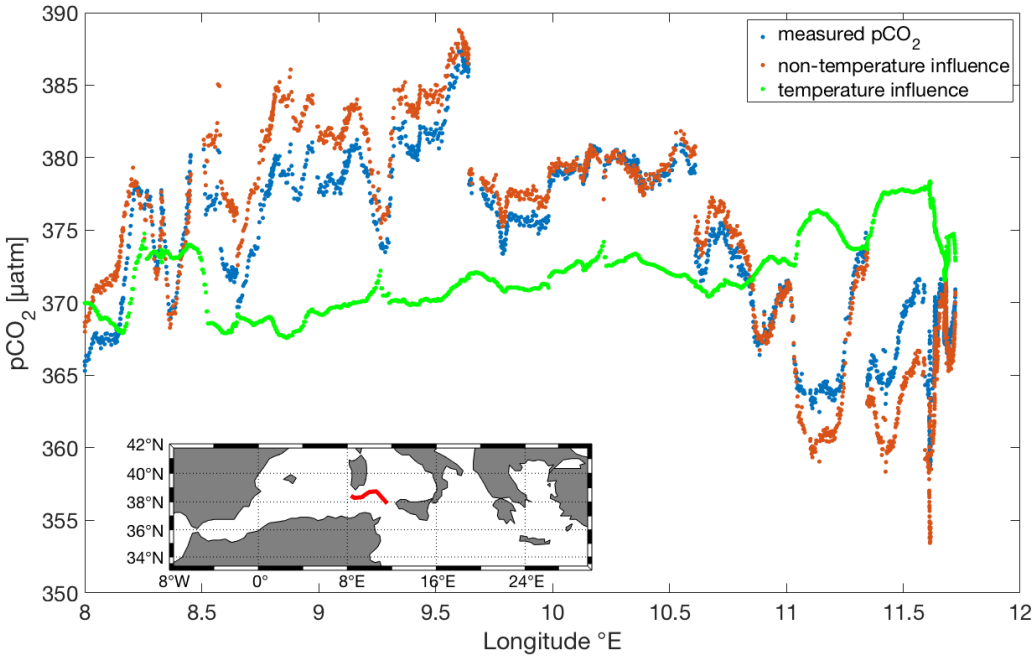

Figure 41: Temperature and non-temperature dependent effects on pCO_2. The values were plotted against the longitude in this zonal section of the Tyrrhenian Sea. The blue data show the measured pCO_2 values, the green data are the calculated pCO_2 values when only a temperature influence is considered and the red show pCO_2 values calculated with a mean temperature of the entire section, i.e. when a specific temperature influence is not considered.

The oxygen saturation in this part of the Mediterranean Sea is shown in figure 42. It reveals that oxygen was or had been consumed at longitudes close to and inside the Strait of Sardinia, also indicating that older upwelling water masses such as the LIW, where oxygen is consumed and CO_2 produced during its travel through the eastern basin at lower depth, could contribute to the surface pCO_2 values by mixing with the AW.

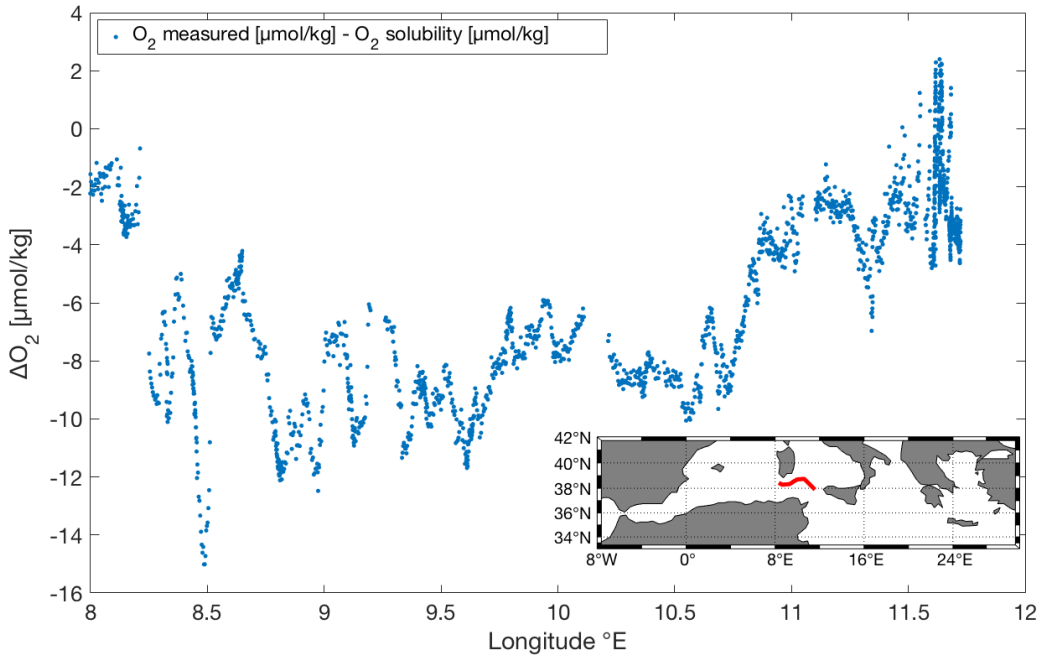

Figure 42: Oxygen saturation calculated from measured oxygen minus oxygen solubility inside the second, zonal section of the Tyrrhenian Sea displayed in µmol/kg and plotted against the longitude.

The mixed layer depth in the Strait of Sardinia was at 100 to 150 m (see figure 29) during the time of the cruise and the shallowest part of the Strait only has a depth of approximately 100 m. Thus, an upwelling of LIW is expected and could affect the partial pressure of CO_2 measured at the surface.

3.3.3 Western Mediterranean basin

A detailed presentation of the pCO_2 values in the zonal section of the Western Mediterranean basin, from the Strait of Sardinia (longitude: 8 °E) to the Strait of Gibraltar (longitude: 5 °W), is shown in figure 43. This section covered a latitude ranging from 38.5 °N to 36 °N.

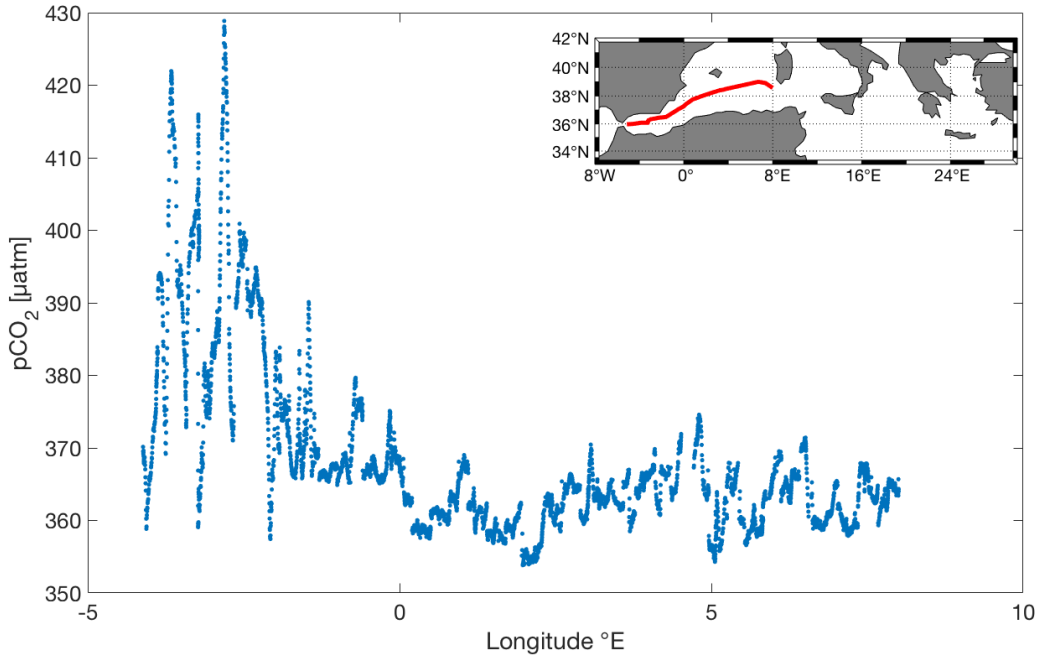

Figure 43: Measured pCO_2 in the western basin of the Mediterranean Sea plotted against the longitude.

Inside the open Western Mediterranean, between a longitude of 0 °E and 8 °E, the pCO_2 values showed a rather constant level of approximately 365 µatm. However, west of a longitude of 0 °E, in the Alboran Sea, the pCO_2 showed high variations. Overall, it increased by approximately 30 µatm but variations ranged between of 360 and 430 µatm. This was also the only part of the cruise, where the water appeared to be oversaturated when compared to atmospheric pCO_2.

The high variations could be caused by an upwelling of LIW, which is characterized by higher pCO_2 resulting from oxygen consuming/pCO_2 producing organisms and a mixing with CO_2-rich deep water masses. As discussed above, the water mass (LIW) moves towards the Atlantic and, due to the shallow water depth in the Strait of Gibraltar upwells at these longitudes.

Figure 44 shows the influences of temperature and non-temperature effects on the significant pCO_2 increase in the Alboran Sea revealing a dominance of non-temperature effects. However, the influence is rather minor in the central western basin (longitudes 0 °E to 8 °E) indicating that air-sea gas exchange was the main contributor to the measured pCO_2 in this part.

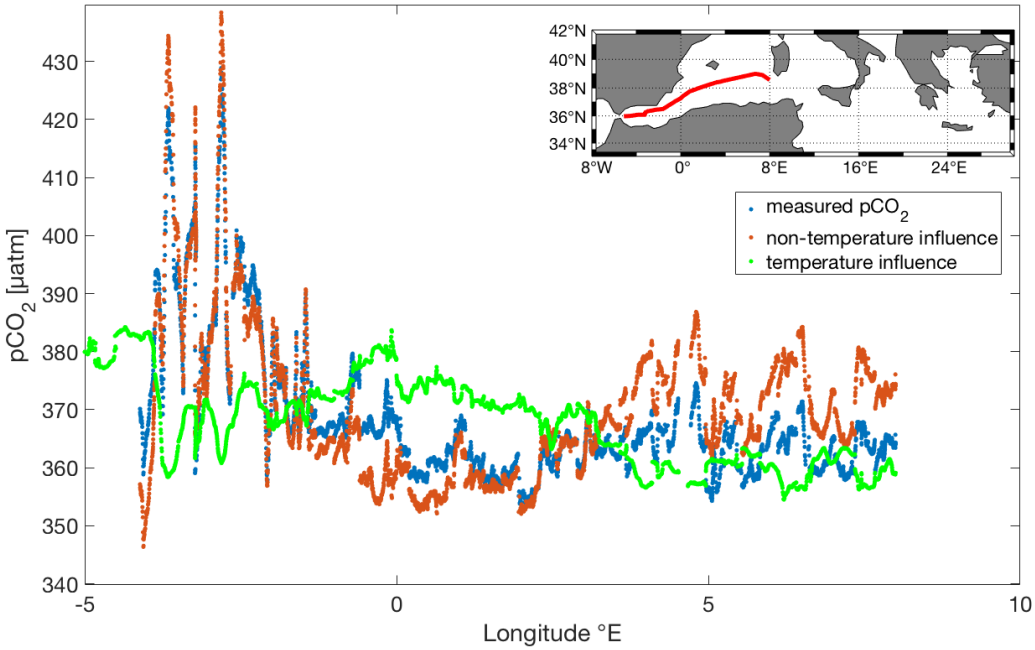

Figure 44: Temperature and non-temperature dependent effects on pCO_2. The values were plotted against the longitude in the Western Mediterranean basin. The blue data show the measured pCO_2 values, the green data are the calculated pCO_2 values when only a temperature influence is considered and the red show pCO_2 values calculated with a mean temperature of the entire section, i.e. when a specific temperature influence is not considered.

Apart from upwelling LIW, another factor possibly responsible for the increase and variation of pCO_2 in the Alboran Sea could be a mixing of the AW newly entering from the Atlantic with older AW that had circulated through the western basin of the Med. As discussed above, a branch of AW, which separated from the eastward-moving main part inside the Tyrrhenian Sea, returns towards the Strait of Gibraltar after crossing the Tyrrhenian and Balearic Seas. During this movement, pCO_2 increases in this water mass most likely due to (1) general air-sea gas exchange as the water is mainly undersaturated in CO_2, (2) mixing with LIW in the Gulf of Lyon and (3) travelling along the coastline of France and Spain, which increases the likelihood of organic CO_2 production.

As already reported by Palmiéri et al (2015), the Alboran Sea is a part of the Med where high fluxes occur. This is caused by two anticyclonic eddies that move water masses and could be the reason for high fluctuations observed.[48] Finally, this part of the zonal section is the closest to land and generally coastal waters display higher pCO_2 values.

Oxygen saturation along this section of the cruise is displayed in figure 45. It shows relatively low oxygen levels in the Alboran Sea indicating that oxygen was or had been

consumed in this area (longitudes: -4 °E to -1 °E). This is in line with the higher pCO_2 values observed at these longitudes (see figure 43).

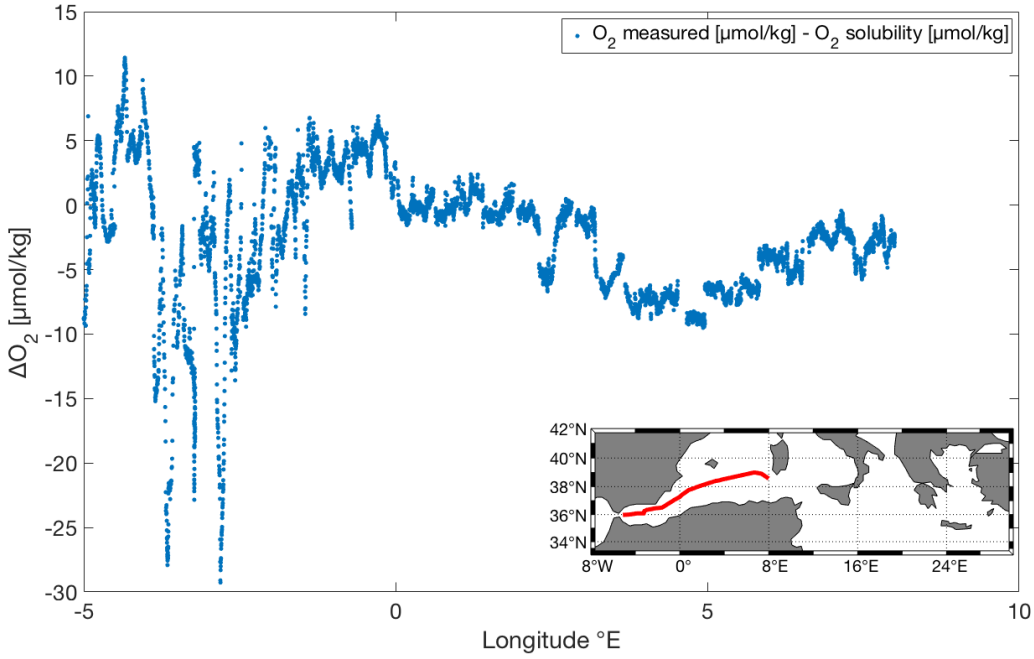

Figure 45: Display of the oxygen saturation calculated from measured oxygen minus oxygen solubility inside the Western Mediterranean basin. Oxygen saturation is given in µmol/kg and plotted against the longitude.

In the following part, the Strait of Gibraltar/Alboran Sea is inspected in even greater detail focusing on the high variations and increasing pCO_2 in this area.

3.3.4 Strait of Gibraltar/Alboran Sea

Of all pCO_2 measurements carried out during cruise MSM 72 those in the Alboran Sea close to the Strait of Gibraltar showed the largest variations. The values ranged from 360 µatm to 430 µatm, with an average at 390 µatm (see figure 46). This part of the zonal section was also the only region where the seawater pCO_2 showed higher values than the atmospheric pCO_2, indicating an oversaturation at some longitudes.

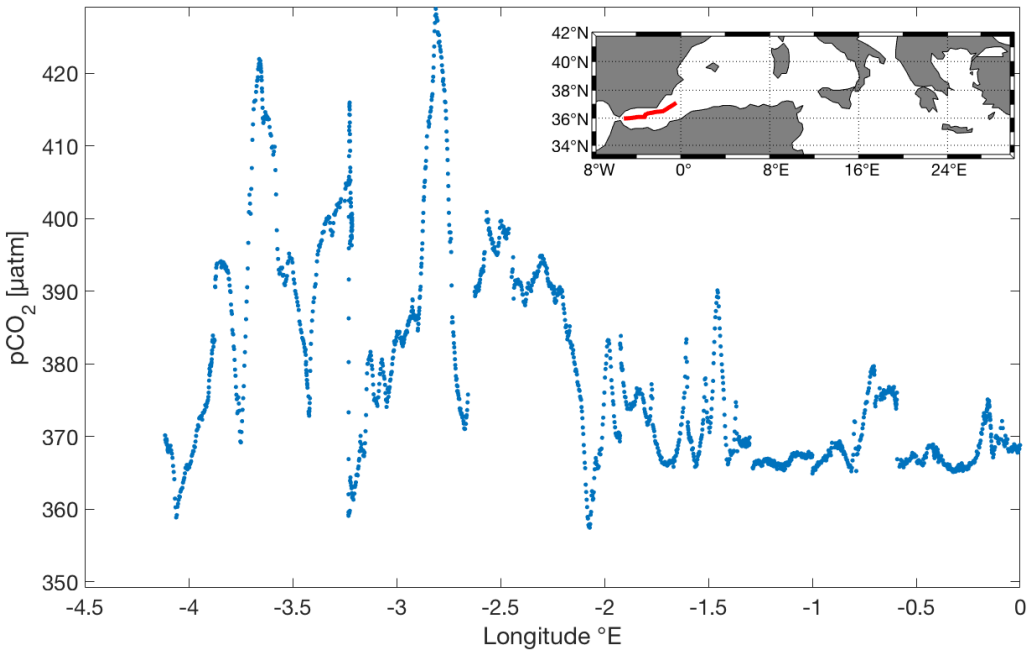

Figure 46: Measured pCO_2 in the Alboran Sea plotted against the longitude.

As discussed in chapter 3.3.3, temperature and non-temperature dependent effects could have caused the high pCO_2 values and variations. To distinguish between these possibilities, the two parameters were again considered separately. Figure 47 reveals that the changes in measured pCO_2 values were mainly caused by non-temperature influences.

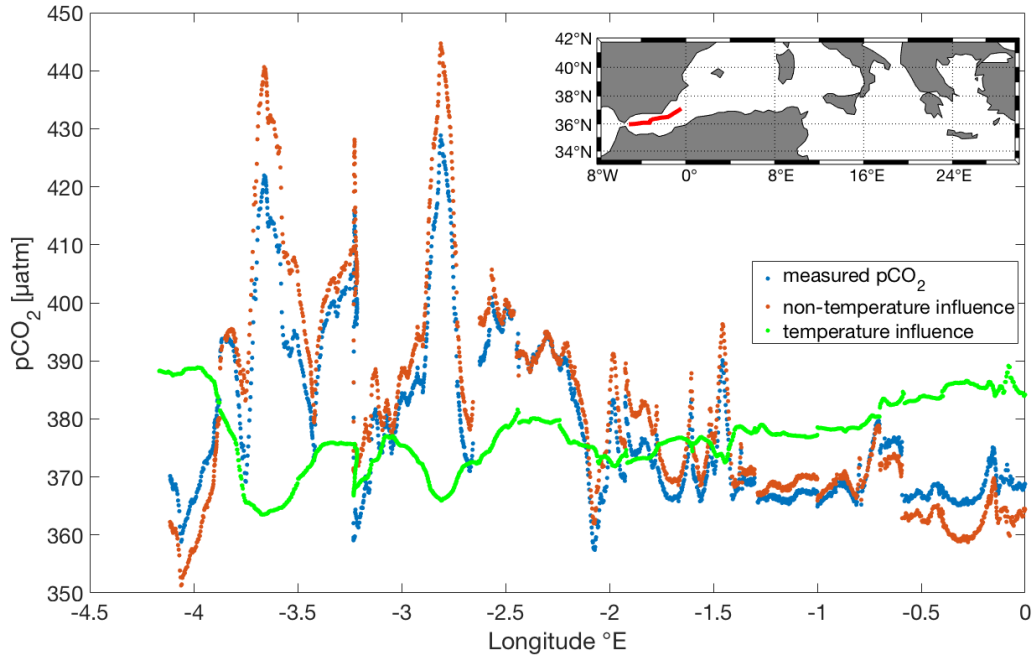

Figure 47: Temperature and non-temperature dependent effects on pCO_2. The values were plotted against the longitude in the Alboran Sea. The blue data show the measured pCO_2 values, the green data are the calculated pCO_2 values when only a temperature influence is considered and the red show pCO_2 values calculated with a mean temperature of the entire section, i.e. when a specific temperature influence is not considered.

As discussed before, these could be attributed to the upwelling of LIW at these longitudes as the water depth decreases. Moreover, influences from the coastal regions have to be considered as the cruise sailed relative close to the African and European coasts and a higher number of CO_2 producing organisms in coastal water is expected. Finally, anticyclonic eddies are present at these longitudes and could cause higher pCO_2 values as already discussed in chapter 3.3.3. The satellite image of the Alboran Sea taken at the time of the cruise (see figure 48) indeed shows the presence of different currents and possibly Eddies that could have affected the surface pCO_2 values during the time of the cruise.

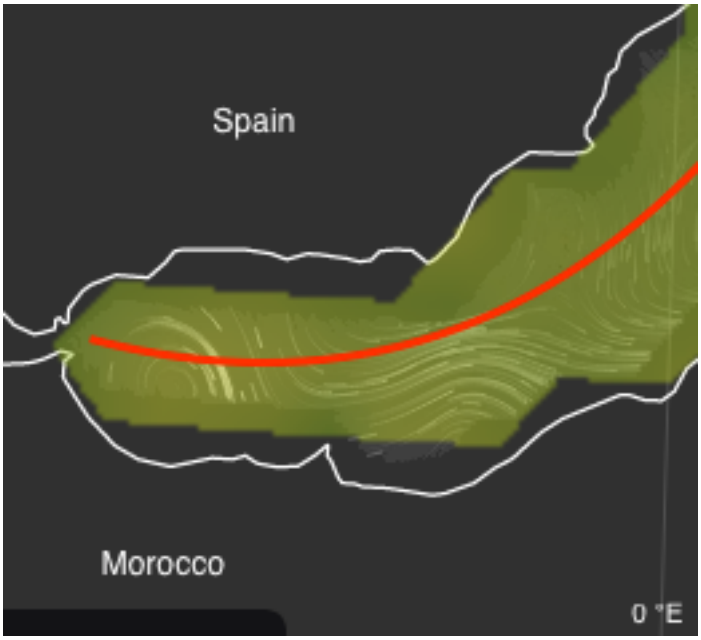

Figure 48: Satellite picture of currents occurring in the Alboran Sea during the time of the cruise (31st of March 2018) taken from https://earth.nullschool.net.[39] The cruise track through the Alboran Sea is depicted as a red line.

Counteracting such CO_2-elevating effects could be organisms such as phytoplankton that consume CO_2 and produce oxygen. Interestingly, a bloom of such organisms is typically observed at these longitudes in spring (El Hourany et al., 2019). However, the relatively high pCO_2 values measured during the cruise indicate that the surface CO_2-elevating effects mentioned above dominated or that the bloom had not occurred until the end of March when the pCO_2 data were recorded during the cruise.[4] In fact, the oxygen saturation data revealed no indication for a phytoplankton bloom as they showed that oxygen rather was or had been consumed (see figure 49).

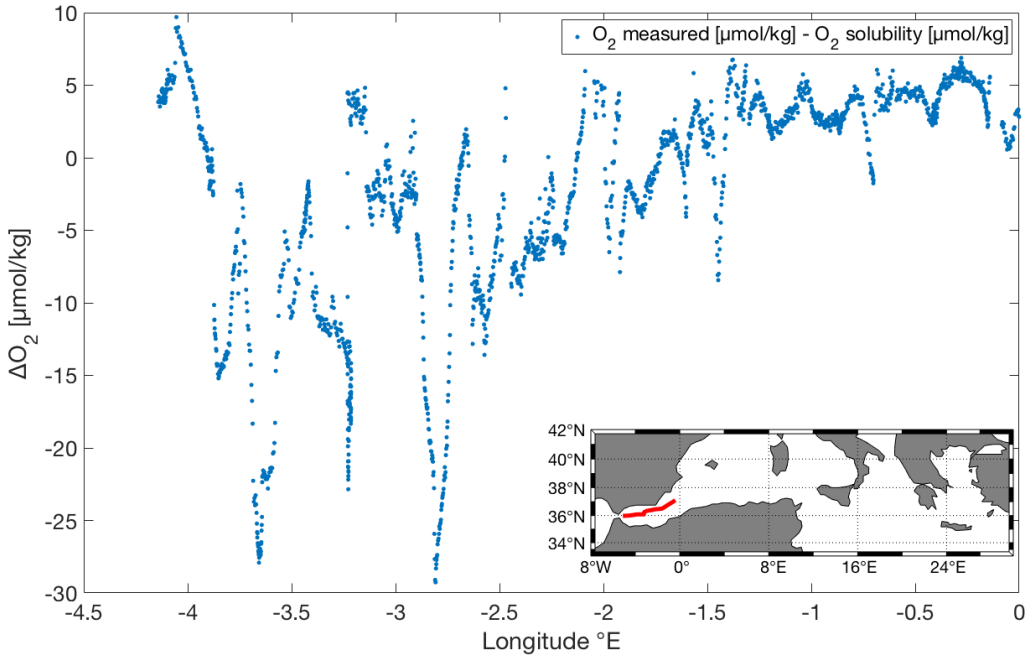

Figure 49: Display of the oxygen saturation calculated from measured oxygen minus the oxygen solubility in the Alboran Sea. Oxygen saturation is given in µmol/kg and plotted against the longitude.

3.3.5 Summary of the detailed pCO_2 analysis in the separated zonal sections

As also discussed in chapter 3.2, the pCO_2 values stayed rather constant in the open sea inside the Western and Eastern Mediterranean basins themselves. Higher variations were seen in the Straits, as the depth of the water column decreased and landmasses are closer to the measuring stations and the ship's cruise. Here the mixing of water masses with different pCO_2 levels, effects of CO_2-producing organisms that live in coastal waters and possibly also the intake of fresh water with different pCO_2 have to be considered.
During this cruise, the pCO_2 values recorded inside almost the entire Med were lower than the atmospheric levels and not in equilibrium. As shown in figure 28, this is common for the time of year when the cruise took place. The general undersaturation could be due to the fact that more CO_2 is biologically fixed by photosynthetic organisms at this time of year and/or transported quickly into the deep ocean as postulated in Miquel et al. (2011). This fast fixation and transport to the deep sea (increasing sink) results in decreased pCO_2 levels at the surface, when the air-sea gas exchange is not sufficient for compensation.[45] Also, the inflowing water from the Eastern Atlantic Ocean is generally undersaturated over the entire year as reported in Benson et al. (2014).[49]

4. Conclusion

The analysis of the pCO_2 data obtained during cruise MSM 72 revealed for most parts of the Mediterranean Sea (Med) a general undersaturation of the surface water in comparison to the CO_2 concentration in the atmosphere. When compared to data recorded in previous years (see figure 28), undersaturation is a common phenomenon for the time of year in which the data were monitored during MSM 72 (March). The opposite, a pCO_2 oversaturation, had been reported for the Med surface waters in the summer months indicating that parameters affecting the pCO_2 levels (air-sea gas exchange, currents, winds, organic CO_2 production vs. consumption and others) differ between the seasons. The general overview of the zonal section (see figure 27) showed that pCO_2 remains relatively constant in the main basins, the Eastern and Western Mediterranean basin, and that slightly lower pCO_2 values prevail in the central Western as compared to the central Eastern Med. Several parameters could contribute to these relatively subtle differences, for example differences in the air-sea gas exchange, differences in temperature and/or different rates in organic CO_2 production vs. consumption. As compared to the larger basins, higher variations occurred inside the Straits and Channels, probably due to a significant upwelling of deeper water masses in these relatively shallow areas. The upwelling leads to a mixing of water masses that is most likely responsible for higher variations in pCO_2. Moreover, it will cause increased pCO_2 values because water masses from the interior carry higher amounts of CO_2 due to the absence of CO_2 consuming organisms that rely on light-driven photosynthesis.

A more detailed analysis showed that temperature and non-temperature influences affect the pCO_2 differently in different parts of the Med. Prominent examples were the Otranto Strait, where a temperature decrease appeared to have caused the pCO_2 reduction at a latitude of 40 °N (see figure 24), and the Sardinia Channel and Strait of Gibraltar, where predominantly non-temperature effects led to an increase in pCO_2 (see figures 41&44). Such non-temperature influences are most likely vertical mixing of upwelling deep or intermediate water masses, for example the LIW, which carry higher concentrations of CO_2. Currents or eddies present close to the Straits during the time of the cruise could also contribute to vertical upwelling and support a more significant mixing of different water masses. These factors also cause local variations in the pCO_2

values, which were particularly evident in the Alboran Sea close to the Strait of Gibraltar at longitudes of 0 °W to 5 °W (see figure 47).

5. Outlook

The data recorded during cruise MSM 72 have revealed the highest pCO_2 variations in the different straits. Thus, some future emphasis should be put on these areas to assess whether such variations are a specific feature of shallow waters with relatively large currents. For example, it could be analyzed whether these variations are observed throughout the year or only at specific times when the MLD is rather large (100-200 m) and upwelling water masses affect the surface measurements. A measuring station inside the Alboran Sea/Strait of Gibraltar operating year-round could deliver results on this. A similar year-round recording of pCO_2 in the other straits, and for comparison also other parts of the Med, could deliver valuable information on the effect of the seasons on pCO_2 variations. Furthermore, to visualize how pCO_2 in the Med changes in the future, cruises recording pCO_2 should cross the Med along the same sections and at the same time of year (March) in five or ten years and thus reveal data that could be compared directly.

pCO_2 recordings of surface seawater, not only inside the Mediterranean Sea but also in other oceans with much larger water masses, will be of importance in the future to visualize the impact of rising atmospheric pCO_2 on the ocean. It can be expected that surface water pCO_2 will continue to increase in the following years but to what extent does this happen and what differences might exist between different oceans? Furthermore, by relating the pCO_2 data to ocean currents, eddies and the respective MLD, it should be possible to assess whether upwelling water masses generally lead to a further increase of pCO_2 at the surface. And, very important for organisms living in the ocean, to what extent will the increasing pCO_2 levels affect the ocean pH and thus conditions for life? These questions can only be answered with direct measurements of atmospheric and surface water pCO_2 in as many parts of the world's oceans as possible.

Literature

1. MSM 72 Final Cruise Report.

2. MSM 72 Weekly report Week01.

3. https://www.goruma.de/erde-und-natur/weltmeere/mittelmeer (**05.11.2019**).

4. R. E. Hourany, M. A. Saab, G. Faour, C. Mejia, M. Crépon, S. Thiria, *Journal of Geophysical Research: Oceans*, **2019**, 124, 5827-5843.

5. T. Tanhua, D. Hainbucher, K. Schroeder, V. Cardin, M. Alvarez, G. Civitarese, *Ocean Science*, **2013**, 9, 789-803.

6. A. Schneider, T. Tanhua, W. Roether, R. Steinfeldt, *Ocean Science*, **2014**, 10, 1-16.

7. M. Alvarez, H. Sanlean-Bartolome, T. Tanhua, L. Mintrop, A. Luchetta, C. Cantoni, K. Schroeder, G. Civitarese, *Ocean Science*, **2014**, 10, 69-92.

8. B. Alhammoud, K. Beranger, L. Mortier, M. Crepon, I. Dekeyser, *Progress in Oceanography*, **2005**, 552, 1-22.

9. https://www.seilnacht.com/Chemie/ch_co2.htm (**04.11.2019**).

10. https://www.lufft.com/blog/fuenf-gruende-warum-die-ueberwachung-der-co2-konzentration-eine-gute-idee-ist/ (**03.02.2020**).

11. https://energyeducation.ca/encyclopedia/Anthropogenic_carbon_emissions (**03.02.2020**).

12. http://www.weltinnenpolitik.net/wp-content/uploads/2018/06/1_Das_Menschheitsexperiment-249-960-10000-80.png (**04.11.2019**).

13. B. Jähne, E. Monahan, *Air-Water Gas Transfer*, AEON Verlag, **1995**, 375-383.

14. R. Wanninkhof, W. E. Asher, D. T. Ho, C. Sweeney, W. R. McGillis, *Annu. Rev. Mar. Sci.*, **2009**, 1, 213-244.

15. A. Körtzinger, U. Riebesell, *Current Topics in marine biogeochemistry I (bioc-231) – air-sea exchange*, Vorlesung, **2018**.

16. P. Rivaro, R. Messa, C. Lanni, E. Magi, G. Budillon, *Polar Research*, **2014**, 33, 20403.

17. A. G. Dickson, *The carbon dioxide system in seawater: equilibrium chemistry and measurements*, **2010**, 17-40.

18. R. E. Zeebe, D. A. Wolf-Gladrow, *CO2 in Seawater: Equilibrium, Kinetics, Isotopes*, edition 3, Elsevier Oceanography Series, **2005**, 65, 5.

19. J. L. Sarmiento, N. Gruber, *Ocean Biogeochemical Dynamics*, Princeton University Press, **2006**.

20. A. Körtzinger, U. Riebesell, *Current Topics in marine biogeochemistry I (bioc-231) – Marine CO_2 system*, Vorlesung, **2018**.
21. K. M. Johnson, K. D. Wills, D. B. Butler, W. K. Johnson, C. S. Wong, *Mar. Chem.*, **1993**, 44, 167-187.
22. A. G. Dickson, C. L. Sabine, J. R. Christian, *Guide to best practices for Ocean CO2 Measurements*, Pices Special Publication 3, **2007**, IOCCP Report No. 8.
23. http://mariscope.com.ar/files/products/files/HydroCCO2SpecSheet_201703271323-filename.pdf (**30.07.2019**).
24. https://www.kongsberg.com/maritime/products/mapping-systems/Chemical-Sensors-and-Analyzers/HydroC-CO2/ (**03.07.2019**).
25. https://webbook.nist.gov/cgi/cbook.cgi?ID=C124389&Units=SI&Type=IR-SPEC&Index=1#IR-SPEC (**29.07.2019**).
26. H. Lui, A. C. A. Chen, *Limnol. Oceanogr.: Methods 15*, **2017**, 328-335.
27. TD 269 Operating Manual Oxygen Optode 4330.
28. C. Lagdon, *Determination of dissolved oxygen in seawater by winkler titration using the amperometric technique*, IOCCP Report No. 14, ICPO publication series N134, **2010**.
29. M. C. Patsavas, R. B. Byrne, B. Yang, R. A. Easley, R. Wanninkhof, X. Liu, *Marine Chemistry*, **2015**, 168, 80-85.
30. Data Precessing for Contros HydroC CO_2 sensor sheet (**07.11.2019**).
31. P. Fietzek, B. Fiedler, T. Steinhoff, A. Körtzinger, *Journal of Atmospheric and Oceanic Technology*, **2014**, 31, 181-196.
32. Ocean Data Standards – Recommendation for a Quality Flag Scheme for the Exchange of Oceanographic and Marine Meteorological Data, *IOC Manuals and Guides*, 54, **2013**, Vol. 3, Version 1.
33. S. van Heuven, D. Pierrot, J. W. B. Rae, E. Lewis, D. W. R. Wallace, *MATLAB Program Developed for CO2 System Calculations. ORNL/CDIAC-105b. Carbon Dioxide Information Analysis Center, Oak Ridge National Laboratory, U.S. Department of Energy, Oak Ridge, Tennessee*, **2011.**
34. T. J. Luecker, A. G. Dickson, C. D. Keeling, *Mar. Chem.*, **2000**, 70, 105-119.
35. A. G. Dickson, *Jounal, of Chemical Thermodynamics*, **1990**, 22, 113-127.
36. J. C. Orr, J.-M. Epitalon, A. G. Dickson, J.-P. Gattuso, *Routine uncertainty propagation for the marine carbon dioxide system*, *Mar. Chem.*, **2018**.
37.https://www.esrl.noaa.gov/gmd/dv/iadv/graph.php?code=LMP&program=ccgg&type=ts (**01.12.2019**).

38. T. Takahashi, S. C. Sutherland, C. Sweeney, A. Poisson, N. Metzl, B. Tillbrook, N. Bates, R. Wanninkhof, R. A. Feely, C. Sabine, J. Olafsson, Y. Nojiri, *Deep-Sea Research II*, **2002**, 49, 1601-1622.

39. https://earth.nullschool.net/#current/ocean/surface/currents/overlay=sea_surface_temp/orthographic=-349.21,37.80,2718 (**03.02.2020**).

40. H. R. Powley, M. D. Krom, P. Van Cappellen, *American Geophysical Union*, **2017**, 31, 1010-1031.

41. A. Schneider, T. Tanhua, A. Körtzinger, D. W. R. Wallace, *Journal of Geophysical Research*, **2010**, 115, C12050.

42. https://www.socat.info/index.php/data-access/ (**31.01.2020**).

43. http://www.ifremer.fr/cerweb/deboyer/mld/Surface_Mixed_Layer_Depth.php (**08.01.2020**).

44. L. G. Anderson, A. Olsen, *Geophysical Research Letters*, **2002**, 29 (17), 1835.

45. J.-C. Miquel, J. Martin, B. Gasser, A. Rodriguez-y-Baena, T. Toubal, S. W. Fowler, *Progress in Oceanography*, **2011**, 91, 461-481.

46. L. Nykjaer, *Climate Research*, **2009**, 39, 11-17.

47. A. J. Sutton, R. A. Feely, S. Maenner-Jones, S. Musielwicz, J. Osborne, C. Dietrich, N. Monacci, J. Cross, R. Bott, A. Kozyr, *Earth System Science Data Discuss*, **2018**, 77, 1-23.

48. J. Palmiéri, J. C. Orr, J.-C. Dutay, K. Béranger, A. Schneider, J. Beuvier, S. Somot, *Biogeosciences*, **2015**, 12, 781-802.

49. N. U. Benson, O. O. Osibanjo, F. E. Asuquo, W. U. Anake, *International Journal of Marine Science*, **2014**, 4 (72), 1-7.

Acknowledgements

First of all, I want to thank Prof. Dr. Arne Körtzinger for offering the possibility to write this thesis in his department, and Prof. Dr. Hermann Bange for being my second reviewer.

I would also like to thank the entire CO_2 group for the help and a great working atmosphere during the time of this master thesis. Special thanks go to Dr. Tobias Steinhoff and Dr. Toste Tanhua (Transient Tracer group) for their support and helpful discussions.

The courses in chemical oceanography really sparked my interest in this science. Therefore, I am grateful to my course lecturers Prof. Dr. Arne Körtzinger, Prof. Dr. Hermann Bange and Prof Dr. Ulf Riebesell.

Also, I want to thank all the scientists and ship members of the cruise MSM 72 for a productive working environment and an interesting experience.

A special thank you to my family, who supported my education and my decision to study this science.

Last but not least, I would like to thank all my fellow students and especially my long time roommates Lennert and Stephan for a great living and studying atmosphere.

Eidesstattliche Erklärung

Hiermit versichere ich, Lennart Gerke, an Eides statt, dass ich diese vorliegende Arbeit zum Thema “pCO2 in the Mediterranean Sea during the cruise MSM 72”, selbständig und ausschließlich mit den angegeben Quellen und Hilfsmitteln angefertigt habe.

Ort, Datum _____